FABRICATION OF PHOTONIC DEVICES ON LITHIUM-NIOBATE-ON-INSULATOR (LNOI) CHIPS

SOHAM SATAPARNO SAHA

(B. Eng. (Hons.)NUS)

A THESIS SUBMITTED

FOR THE DEGREE OF MASTER OF ENGINEERING

DEPARTMENT OF ELECTRICAL AND COMPUTER ENGINEERING

NATIONAL UNIVERSITY OF SINGAPORE

2015

DECLARATION

I hereby declare that the thesis is my original work and it has been written by me in its entirety. I have duly acknowledged all the sources of information which have been used in the thesis.

This thesis has also not been submitted for any degree in any university previously.

Soham Sataparno Saha

12 Aug 2015

ACKNOWLEDGEMENTS

I wish to acknowledge and thank all the people who have encouraged and supported me throughout the pursuit of this degree.

Firstly, I would like to thank my supervisor, Prof. Mankei Tsang, for providing me with this research opportunity. His ideas, support and encouragement were essential in the progress of the research project. I would also like to thank Prof. Aaron Danner, who helped me gain access to the laboratory resources I required for the fabrication of the devices, and helped me understand many of the physics-related aspects of the project.

Siew Shawn Yohanes, my laboratory partner and a dear friend, is the person whom this project would not have completed without. His perseverance and positive attitude were the fuel that drove our project forward.

Technical support and lab safety were two vital factors of the project. I would like to thank Dr. Liao Baochen, the laboratory coordinator, who made my work in the cleanrooms safe and enjoyable.

The research was supported by a grant from NRF, Singapore.

I would also like to thank my colleagues Deng Jun, Ranjith, Shan Zeng, and Shi Lin, for creating a motivating, enjoyable and productive atmosphere, throughout and beyond the timeline of my stay in NUS.

Finally, I would like to thank my parents and my brother, who have always been there for support. I thank my sister, Shinjini, for making a trip to Singapore during her summer vacation, and putting up with me during the stressful times of my thesis write-up.

CONTENTS

SUMMARY

The high electro-optic and nonlinear coefficients of lithium niobate make it a highly promising material for optical modulator design, cavity quantum electrodynamics experiments, and microwave photonics. The two most common techniques for photonic device fabrication on lithium niobate are titanium diffusion and proton exchange. However, due to a very low refractive index contrast between the waveguiding region and the surrounding material, the waveguides formed through these processes have low mode confinement, high bending losses, and are often polarization dependent, making it difficult to fabricate compact photonic structures on the material.

This thesis describes the fabrication techniques developed and optimized to produce low-loss waveguides and resonators in lithium-niobate-on-insulator (LNOI) chips. LNOI chips comprise a thin film of lithium niobate adhering on an insulating substrate like silicon dioxide. Devices fabricated on LNOI through etch-based techniques provide good mode confinement because of the high index contrast between the waveguiding and cladding regions. Also, because of the smaller waveguide widths attainable, a greater control of the critical dimensions of devices is possible.

Optical waveguides, power splitters, and microring resonators were fabricated on lithium-niobate-on-insulator chips, with robust fabrication techniques, namely electron beam lithography (EBL) and ion-beam etching. The structures have been characterized in terms of propagation loss, extinction ratio, and quality factor. The fabricated structures showed good performance, and the fabrication techniques have the potential to be used in the mass manufacture of compact lithium niobate based optical devices.

LIST OF FIGURES

1. INTRODUCTION

1.1 Lithium Niobate in Literature: Lithium Niobate and its Applications in Nonlinear Optics

The drive for research in nonlinear optics arose from its enormous potential for application in several fields, including, but not limited to communications, lasers, and quantum optics [1].

Nonlinear optical materials were first used for the generation of lasers at new frequencies not available with existing laser sources, through parametric up and down conversion [2]. But the application of nonlinear optics soon pervaded other areas of science and technology. The next paragraph highlights some of the most common applications of nonlinear optical phenomena.

The most common nonlinear processes are harmonic generation, frequency mixing, optical parametric oscillation, and Raman shifting. Harmonic generation is commonly used in lasers. Nonlinear optical effects have been used in optical transmission systems to cancel the dispersion and diffraction of light to produce temporal and spatial optical solitons. Nonlinear optical devices are also an essential component in research in optical computing. The advantages of photonic devices using nonlinear optical processes over electronic devices are faster speed, owing to the use of photons instead of electrons, and higher bandwidth capacity. Nonlinear optical devices such as Mach-Zehnder Interferometers (MZIs) are used in ultrafast data processing.

There are certain requirements for a nonlinear optical material that have to be met in order for it to be suitable for device applications. These criteria are:

adequate nonlinearity and optical transparency, proper birefringence for phase-matching, and sufficient resistance to optical damage by intense optical irradiation.

Lithium niobate (LN) is a transparent electro-optic crystal, with the chemical formula $LiNbO_3$. Due to its high Pockels and Kerr effects, lithium niobate is a suitable candidate for a number of experiments in nonlinear optics ranging from sum and difference frequency generation to microwave photonics. In fact, it was one of the first materials on which parametric oscillations had been demonstrated. These attributes propelled LN to the forefront of materials used in various electro-optical and nonlinear optical applications. It is also commercially used in the fabrication of high-speed modulators such as Mach Zehnder interferometers (MZIs) for ultrafast data transfer.

Lithium niobate is birefringent, with an ordinary index of 2.28 (in the x and y orientations) and an extraordinary index of 2.18 (in the z orientation) at a wavelength of 633nm [3]. At a wavelength of 1600nm, the ordinary refractive index is 2.21, and the extraordinary index is 2.13.

$$\begin{pmatrix} 0 & -3.4 & 8.6 \\ 0 & 3.4 & 8.6 \\ 0 & 0 & 30.5 \\ 0 & 28 & 0 \\ 28 & 0 & 0 \\ -3.4 & 0 & 0 \end{pmatrix}.$$

Figure 1. Pockels effect impermeability tensor

Under an applied electric field, the polarization of the optical fields inside the crystal can change according to the equation,

$$\mathbf{P} = \varepsilon_0\left(\chi^{(1)} \cdot \mathbf{E}(\mathrm{t}) + \chi^{(2)} \cdot \mathbf{E^2}(\mathrm{t}) + \chi^{(3)} \cdot \mathbf{E^3}(\mathrm{t}) + \cdots\right). \quad \text{(Equation 1)}$$

This provides the opportunity to employ lithium niobate in a wide array of nonlinear optical experiments.

The following section provides an overview of the various types of nonlinear optical experiments that have been carried out so far in lithium niobate.

1.1.1 Mach Zehnder interferometers

The electro optic modulation of lithium niobate is well suited for modulation and switching of fast optical communication systems.

A Mach Zehnder Interferometer, or MZI, comprises a power splitter splitting light into two equal sections in its two branches, leading to two output ports. Without a voltage applied (the bar state), light interferes constructively at a particular output port. When a voltage is applied across the arms, due to Pockels Effect, the refractive index of the waveguides changes in a way that causes the light passing through the arms to undergo a relative phase shift of π, causing destructive interference at the initial output port, and constructive interference at the other. This phenomenon can be used in ultrafast optical modulation and switching [4].

MZIs fabricated on lithium niobate by titanium diffusion process are commercially available. However, due to the small index contrast produced by titanium diffusion, they tend to have large bending losses associated with them. In order to circumvent this, the devices have large bends at the input and output ports, causing the typical device to be several centimeters long.

1.1.2 Second harmonic generation

Second harmonic generation is a nonlinear optical phenomenon that occurs due to the $\chi^{(2)}$ nonlinearity in electro-optic crystals. This technique is commonly used as an indicator of the crystal integrity once waveguides have been fabricated on it via diffusion based techniques.

Waveguides formed by proton exchange were seen in previous experiments to have a reduction in their nonlinear coefficients [5]. The coefficients could be recovered by annealing the fabricated structures [6,7].

1.1.3 Experiments with entangled photons

Spontaneous parametric down-conversion can produce entangled photon pairs. In a nonlinear crystal such as lithium niobate, the photons can split into twin photons that are phased-matched and have correlated polarizations. This typically happens at a low conversion efficiency, estimated to be around 1 in 10^{10}. SPDC has been observed in lithium niobate waveguide arrays [8].

If we are able to produce ultra-high Q factor microcavities, we can attempt experiments with entangled photons.

1.1.4 Microwave photonics experiments

In 2001, Cohen and Hossein-Zadeh et al. theorized and experimentally demonstrated a device that could use microwave signals to modulate optical signals [9]. It comprised a lithium niobate disk that was mechanically polished to form a high-Q (4E6) resonator. Light was coupled into it using prism couplers. A microwave resonator was deposited on top of it. Modulation was seen only when the microwave frequency used matched the free spectral range (FSR) of the cavity. Optical modulation was achieved at frequencies reaching

40 GHz, and the experimental results matched closely with theoretical data [10]. In 2002, Ilchenko et. al. carried out a similar experiment on a high-Q whispering gallery mode resonator on lithium niobate, and performed a rigorous theoretical analysis of the results, showing frequency up and down conversions.

1.2 Research Motivation

The high electro-optic coefficients and nonlinear coefficients of lithium niobate make it a highly promising material for optical modulator design, cavity quantum electrodynamics experiments, and microwave photonics. The two most common techniques for photonic device fabrication on lithium niobate are titanium diffusion and proton exchange.

However, due to very low refractive index contrast (usually less than 0.1), the waveguides formed through these processes have low mode confinement, high bending losses, and, are often not polarization independent, making it difficult to fabricate compact photonic structures on the material.

Also, for the fabrication of large, high quality factor (high-Q) cavities for microwave photonics experiments, the conventional way is to mechanically polish a block of lithium niobate. This is suitable for performing experiments in a laboratory set up, but is not a technique that can be used to fabricate optoelectronic devices on a chip.

Lithium-niobate-on-insulator (LNOI) provides a viable solution to the problems. Because of the high index-contrast of the waveguiding regions of rib waveguides in LNOI, they allow for lower bending losses and sharper bends. Also, because of the smaller waveguide widths attainable through etch based

techniques, a greater control of the critical dimensions of devices is possible, enabling the formation of compact interferometers and modulators.

We fabricated and characterized optical waveguides, power splitters, and microring resonators on lithium-niobate-on-insulator chips, employing robust fabrication techniques, namely electron beam lithography (EBL) and ion-beam etching.

As the techniques are further optimized and high – Q resonators are fabricated, experiments in cavity quantum electro-optics and nonlinear optics can be performed on chip [11, 12].

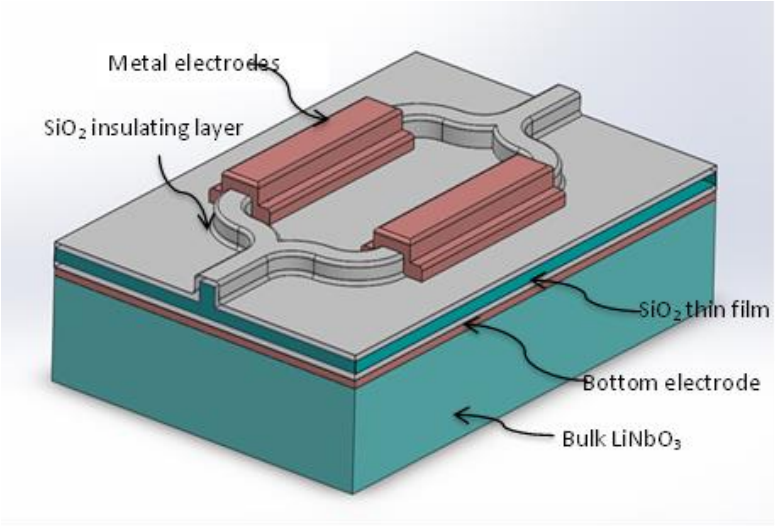

Figure 2. Schematic of a rib waveguide based MZI

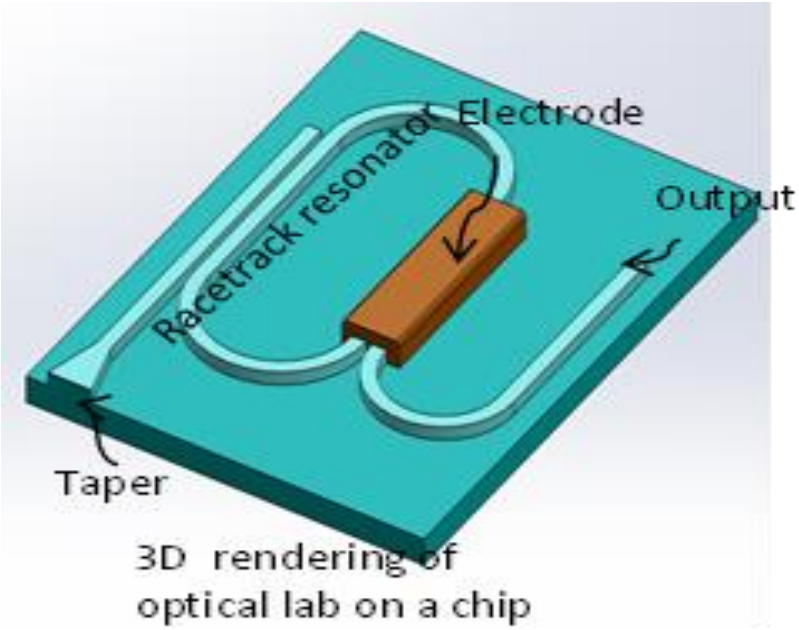

Figure 3. Optical lab on a chip

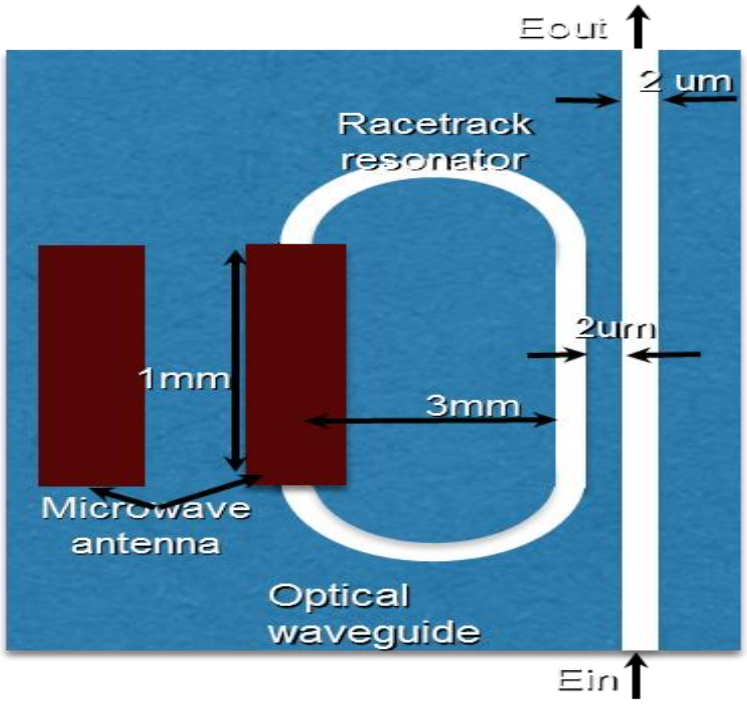

Figure 3. Schematic of a microwave-optical converter

1.3 Thesis Structure

This thesis focuses on the optimization of fabrication parameters for device fabrication on lithium niobate, focusing particularly on lithium-niobate-on-insulator chips.

The thesis is structured in three parts. The first part comprises two major techniques conventionally used to fabricate waveguides and optical devices in lithium niobate: proton exchange, and titanium diffusion. Both these techniques have been rigorously studied in our group for their suitability in quantum optical experiments. The limitations of these techniques is what led to our shift to lithium-niobate-on-insulator devices.

The second section deals with device fabrication on lithium-niobate-on-insulator (LNOI). The section begins with a brief overview of the structure of LNOI chips and their fabrication. Next, the techniques used for processing the chips are described in detail.

The third section follows up with experimental characterization of the devices fabricated using our methods.

Finally, the conclusion summarizes the milestones achieved during the course of the Master's program, and the further work that can be done to demonstrate nonlinear optical phenomena on-chip.

1.4 References

[1] W. Nie, “Optical Nonlinearity: Phenomena, Applications, and Materials,” Advanced Materials, vol. 5, pp. 520–545, (1993).

[2] R. L. Byer, “Nonlinear Optical Phenomena and Materials,” Annual Review of Materials Science, vol. 4, pp. 147-190, (1974).

[3] R. S. Weis and T. K. Gaylord, "Lithium niobate: Summary of physical properties and crystal structure," Applied Physics A, vol. 37, pp. 191-203, (1985).

[4] G.Singh, R.P.Yadav and V.Janyani . “Ti indiffused lithium niobate (Ti: $LiNbO_3$) Mach-Zehnder interferometer all optical switches: A review." New Advanced Technologies, pp. 311-322, (2010).

[5] T. Suhara, H. Tazaki, and H. Nishihara, “Measurements of the reduction in SHG coefficient in LiNbO by proton exchanging,” Electronics Letters, vol. 25, pp. 1326–1328, (1989).

[6] R. W. Keys, A. Loni, and R. M. De La Rue, “Measurement of the increase in the SHG coefficient of proton exchanged LiNbO after annealing using a grating diffraction technique,” Electronics Letters, vol. 26, pp. 625–627, (1990).

[7] X. Cao, R. Srivastava, R. V. Ramaswamy, and J. Natour, “Recovery of second-order optical nonlinearity in annealed proton-exchanged $LiNbO_3$,” IEEE Photonic Technology Letters, vol. 3, pp. 25–27, (1991).

[8] A. S. Solntsev, F. Setzpfandt, A. Wu, D. N. Neshev, A. A. Sukhorukov, Y. S. Kivshar, et al., "Observation of spontaneous parametric down conversion in $LiNbO_3$ waveguide arrays," Lasers and Electro-Optics (CLEO), 2012 Conference on, pp. 1-2, (2012).

[9] D.A. Cohen, M. Hossein-Zadeh, A.F.J. Levi. “High-Q Microphotonic electro-optic modulator.” Solid-State Electronics, vol 45, pp. 1577-1589 (2001).

[10] V. S. Ilchenko, A. A. Savchenkov, A. B. Matsko, and L. M. “Whispering-gallery-mode electro-optic modulator and photonic microwave receiver.” Journal of the Optical Society of America B, vol. 20, issue 2, pp. 333-342, (2002).

[11] M. Tsang. “Cavity quantum electro-optics.” Physical Review A, vol. 81, p. 063837, (2010).

[12] M. Tsang, “Cavity quantum electro-optics. II. Input-output relations between traveling optical and microwave fields,” Physical Review A, vol. 84, p. 043845, (2011).

2. DIFFUSION BASED TECHNIQUES USED TO FABRICATE DEVICES ON LITHIUM NIOBATE

There are three common methods of fabricating waveguides on lithium niobate [1]:

1. Outdiffusion: Outdiffusion of $LiNbO_3$ by high temperature thermal treatments decreases the extraordinary index of the waveguiding region without causing a change in the ordinary index.
2. Indiffusion of metal: Depending on the metal diffused into the substrate, the ordinary and extraordinary indices can both increase or decrease. Titanium diffusion increases the indices by approximately 0.05, making it a suitable technique for waveguide fabrication.
3. Proton exchange: The substrate is dipped in an acid (benzoic acid) where hydrogen ions exchange with Li ions in the substrate. This technique increases the extraordinary index (by approximately 0.1) and decreases the ordinary index.

2.1 Proton Exchange

2.1.1 Mechanism

The proton exchange technique is fairly simple. Benzoic acid, a solid at room temperature, is melted in a glass flask. The crystal is placed in the melt for the desired time, then removed and allowed to cool. Excess benzoic acid can be removed with alcohol. Thermal shock does not appear to be a problem with x-cut crystals, but z-cut crystals occasionally crack during exchange or when they are removed from the melt. The part of the substrate exposed to the molten acid

undergoes a change in the refractive index through the in diffusion of hydrogen ions [2]. Since the ordinary index of the PE region decreases, devices like ring resonators can be only be fabricated in Z-cut LN, and be excited with TM light.

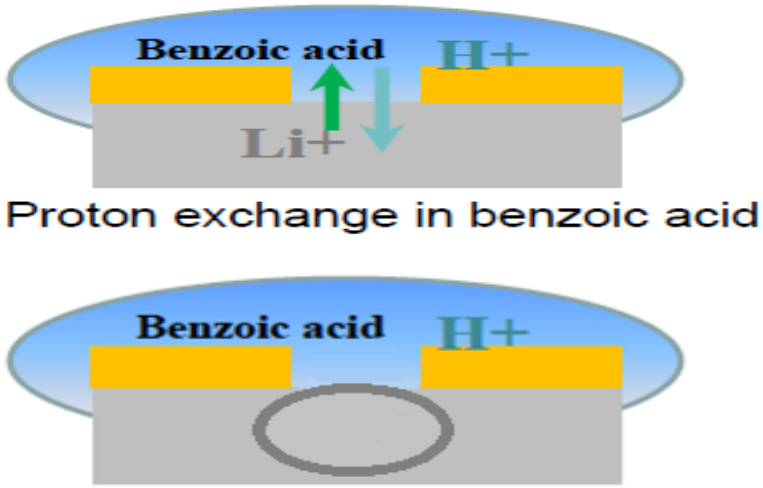

Figure 4. Proton exchange mechanism

Although proton exchanged waveguides have relatively low loss (~1dB/cm), the non-linear coefficients of the material are seen to decrease after the process. A number of approaches report partly contradictory results. The measured SHG efficiencies in both waveguided quasi-phase-matched (QPM) and Cherenkov generation show the nonlinear coefficients in the guiding region to be substantially smaller than that of the untreated $LiNbO_3$ [3]–[8]. The coefficient of PE $LiNbO_3$ waveguides prepared by PE in pure benzoic acid has been measured to vary between 0 and 70% of the bulk value [3-7]. The nonlinear coefficients can be recovered by annealing, as shown in previous investigation [7, 9], and supported by our experiments.

Other techniques of maintaining the non-linear coefficients of the waveguides include PE using diluted benzoic acid (with 3% lithium benzoate) [10] and using vapor phase epitaxy [11]. However, for our experiments, annealed proton exchange (APE) waveguides gave the best results.

An extensive literature study was done to identify the optimal conditions for the fabrication of waveguides with the best parameters. The following table summarizes the findings.

Table 1: Proton exchange and annealing parameters found in literature

Reference	Proton Exchange	Annealing	Phase on the surface (expected)	Nonlinear optic coefficient d33	Wavelength of light used/μm	Loss (dB)
Suhara et al[8]	BA,230°C,2h	-	β_2	0.5± 8	1.06	n.a.
Keys et al. [2]	BA,235°C,1h	0 350°C, 0.5h	β_2 κ_2^{LT-HT}	0.45±0.05 0.65±0.02	-	n.a.
Cao et al. [7]	BA,180°C,1h	0 350°C, 10h	β_2	0.62 0.88	-	n.a.
Laurell et al. [3]	BA,180°C,1h	0 350°C, 10h	β_2 κ_2^{LT-HT}	<0.03 <0.03	1.064	n.a.
Bortz and Fejer [4]	BA,220°C,2h (x-cut)	-	β_1 $\kappa_2^{LT} - \kappa_1^{LT}$	≤0.01	-	n.a.
Bortz et. al. [4]	BA, 173°C,1h	0 333°C,3-63h	β_2	Varies with depth	0.532	n.a.
Hsu et al[5]	BA, 180°C,0.5h	0 300°C,1-17h	β_2	0 0.5	0.532	0.5dB/cm
Raghuram Narayan [11]	BA, 240°C, 0.5h	375°C,2h	-	0dB	-	-
Raghuram Narayan [11] Suchoski et al. [10]	BA, 180°C,5h	375°C,4h	- -	3dB	- -	- 0.15 dB/cm
	BA,180°C, 5h	375°C,8h		0dB		
	BA,240°C,5h	375°C,4h		3dB(cracks propagate)		
	BA,240°C,5h	375°C,8h		0dB(no recovery in certain regions)		
	BA, 200C, 10 min (0.8μm light) 30min (1.55μm)	350°C, 2h 350°C, 4h		-		
J Rams et al [9]	250-375C (vapor phase epitaxy)	-	-	0.9	0.457-1.047	<0.35dB/cm

2.1.2 Process

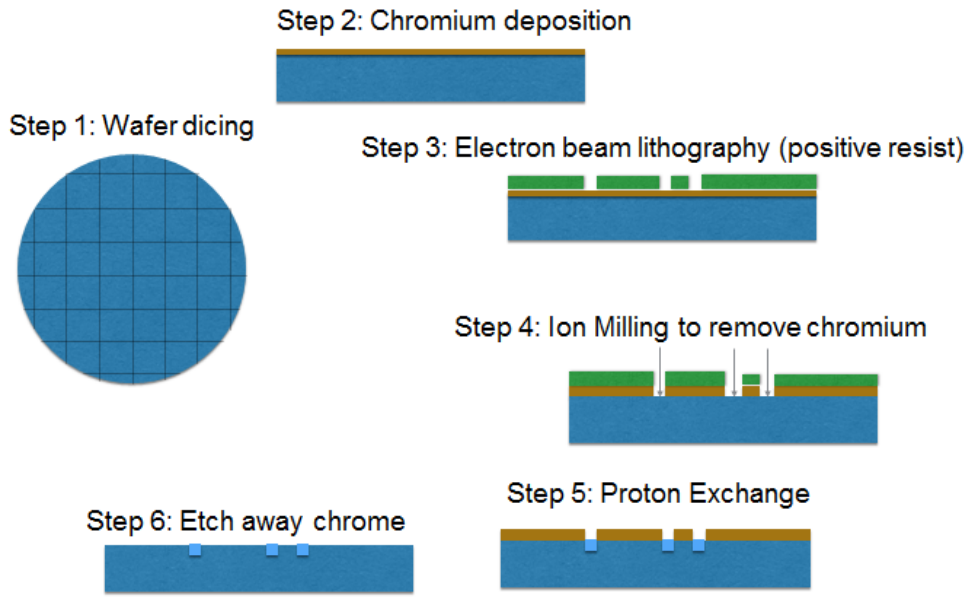

Figure 5. PE channel waveguide fabrication steps

Figure 6 shows the steps in the fabrication of waveguides using proton exchange.

Step 1: Dicing

Using a commercial dicer, the wafer is first diced into 2cm by 2cm blocks. More details about the dicing are provided in section 3.4, which describes the waveguide fabrication procedure on lithium niobate.

Step 2: Chromium deposition

Benzoic acid does not attack most metals. A layer of chromium is used as a hard mask for the proton exchange layer.

The substrate is covered with a 40-50nm layer of chromium, which acts as a conducting layer for EBL. The chromium is deposited using an electron beam evaporator. The layer has to be uniform so that the waveguides have the same height throughout the wafer after the etching.

The deposition is done in a vacuum of 6.0 E -6 Torr, at a rate of 0.1nm/sec, to ensure uniform deposition.

A surface profiler is used to check the final height of the layer after deposition.

Step 3: Electron Beam Lithography with positive resist

PMMA 950K A11 mixed with anisole thinner in a 1:1 ratio is spin coated on the wafers at a speed of 6000rpm for 45 seconds. The sample is baked at 180°C for 90 seconds. In our machine (eLine Plus, Raith), we use a dosage of 200 $\mu C/cm^2$. The solution is then developed in MIBK:IPA in a 1:3 ratio for 50 seconds.

Since our waveguides are about 1 cm in length, in order to minimize the patterning time, a technique called FBMS (Fixed Beam Moving Stage) is used. In this, the beam rotates about its mean position, while the stage is moved under it, exposing the patterned region. Alternatively, photolithography may be used to pattern the waveguides.

Step 4: Ion milling to remove Chromium

Ion milling with Argon ions is used to etch off the exposed chromium layer.

Step 5: Proton exchange

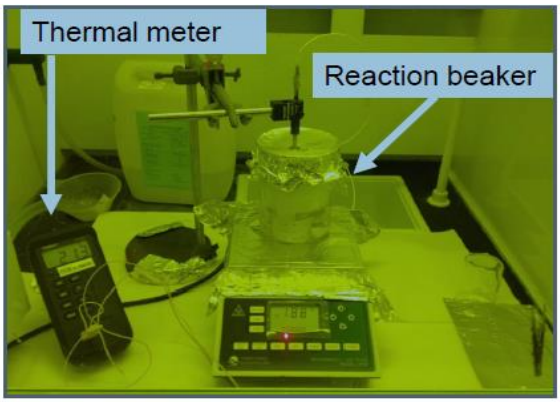

Figure 6. The proton exchange setup

Written below are the exact steps in the fabrication of waveguides through proton exchange. The setup is shown in Figure 7.

The acid area of a fume hood is used for the proton exchange process. The required mass of benzoic acid (solid crystals) is poured into a clean, dry beaker. The beaker is covered with aluminium foil at all times to prevent vapour from escaping. A small hole in punctured in the aluminium to prevent pressure build up, and to take temperature readings using a thermocouple.

The wafer is cleaned using Acetone, IPA and deionized (DI) water, using an ultrasonic cleaner. The cleaning time for each solvent is approximately 5 minutes. The wafer is checked using optical microscope to make sure that the desired patterns are correct and complete.

Benzoic acid is heated to around 230^{o}C using a flash-proof hotplate. The temperature is monitored with a digital thermometer by pricking a hole in the aluminium cover.

Once the temperature has stabilized at the correct settings, the sample is placed in the acid for the required period of time.

After the process, the sample is removed from the acid using acid gloves and teflon tweezers.

The sample is cooled to room temperature and placed in a beaker of acetone for fifteen minutes, to clean residual benzoic acid from the surface. Finally, the sample is cleaned using Acetone, IPA, and DI water.

Step 6: Stripping off the remaining resist and chromium

The remaining photoresist is washed off by acetone. The chromium is washed off by wet etching, using standard chrome-etchant solution. The samples are

subsequently diced to get optically smooth end facets to facilitate the injection of light into the waveguides.

Step 7: Annealing

Annealing is done at 300°C for 2 hours to repair the crystalline defects that build up in the waveguide during proton exchange.

2.1.3 Results

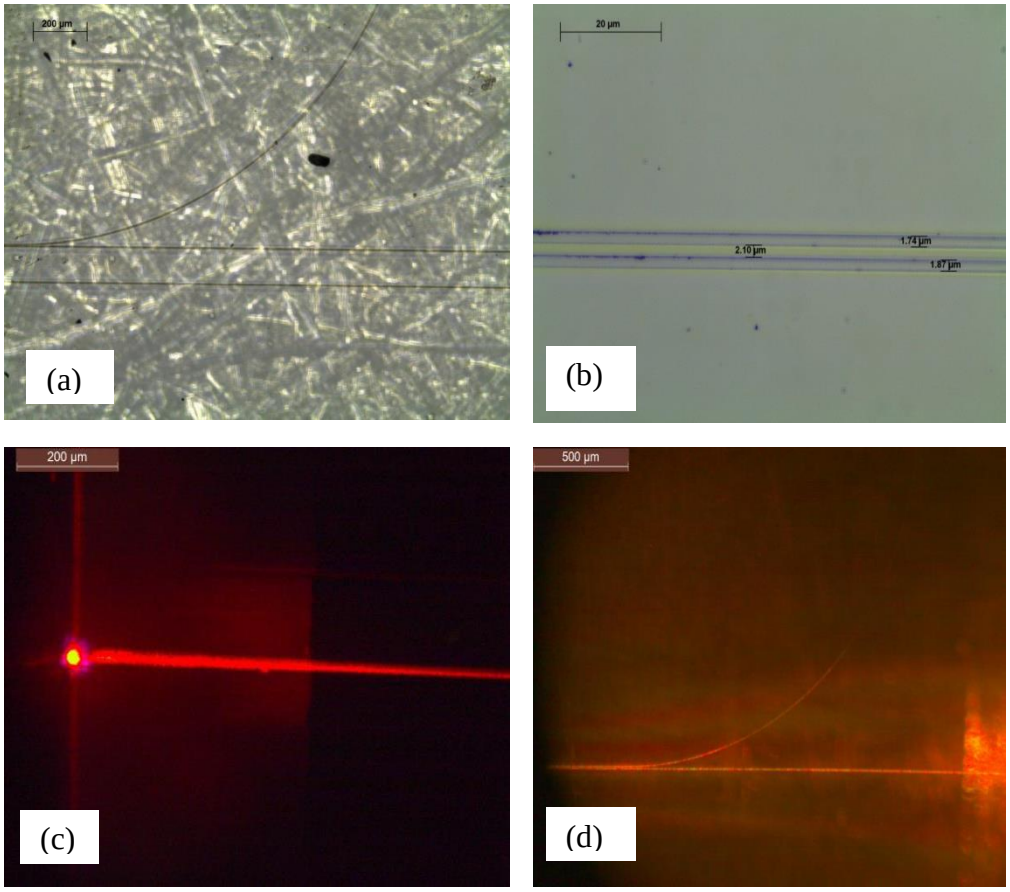

Figure 7. (a) The ring seen under a microscope at 5X magnification; (b) The waveguides at the coupling region; (c) A waveguide illuminated by a broadband laser; (d) Part of the illuminated ring

Large ring resonators were fabricated on proton exchanged lithium niobate samples. When illuminated with a supercontinuum source laser (SuperK Versa, NKT Photonics) centered at 1064nm with a wavelength range of 500nm to 1600nm, the waveguides were seen to couple light. When illuminated with a

1550nm tunable laser source, the waveguides showed a low loss of about 1dB/cm [The measurement technique is discussed in detail in section 3.6.2]. However, possibly because of the low index contrast of the waveguides (~0.02-0.05), the waveguides were seen to have high bending losses [Fig. 8 (d)], and the light did not make it past the large radius bends.

2.1.4 Conclusion for Proton exchange

Several batches of proton exchanged waveguides were fabricated for the project, with propagation losses as low as 1dB/cm, for an input wavelength of 1550nm. At this stage, the bending loss of the PE waveguides could not be measured because even when very large radius bends were designed, the light did not make it past the bends. Due to the high bending losses, we decided not to pursue the technique further.

Although we did not get our desired results from the proton exchanged ring resonators, the experiments gave us a chance to optimize our several of our fabrication steps, such as metal deposition, photolithography, EBL, and ion milling.

During our experiments with proton exchange, we also had a chance to set up our measurement apparatus, which was used for subsequent experiments with titanium diffusion and ion beam etching.

2.2 Titanium Diffusion

2.2.1 Mechanism

Titanium diffusion is commonly used to fabricate waveguides and Mach Zehnder interferometers on lithium niobate.

Titanium diffusion involves depositing titanium on top of the substrate, and heating the substrate (in various different atmospheres) to around 1000°C for 8-12 hours [1], where titanium replaces the lithium sites in the crystal, causing an increase in the index change. Wet oxygen is usually recommended at some stage (usually the last hour) to allow re-oxidation and also prevents lithium ion outdiffusion.

The index contrast introduced by titanium diffusion is smaller than that typically caused by proton exchange, but it increases both the ordinary and the extraordinary indices. Also, Ti diffusion decreases the nonlinear parameters of lithium niobate by a lesser amount.

We investigated the effectiveness of titanium diffusion in the fabrication of waveguides and ring resonators.

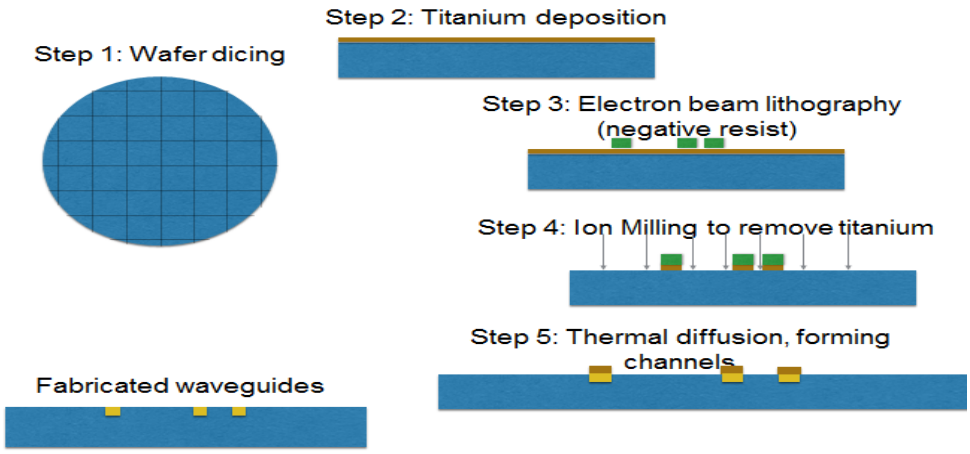

Figure 8. Titanium diffusion work flow

2.2.2 Process

Titanium diffusion follows steps similar to proton exchange.

Step 1: Dicing

Using a commercial dicer, the wafer is first diced into 1cm by 1cm blocks. More details about the dicing are provided in the LNOI waveguide fabrication section.

Step 2: Titanium deposition

A layer of titanium is deposited on the substrate using an electron beam evaporator. The substrate is covered with an 80nm layer of titanium using an electron beam evaporator.

The deposition is done in a vacuum of 6.0 E -6 Torr, at a rate of 0.1nm/sec, to ensure uniform deposition. A surface profiler is used to check the final height of the layer after deposition.

Step 3: Electron Beam Lithography with negative resist

Ma-N 2405 is spin coated on the wafers at a speed of 6000rpm for 45 seconds and subsequently baked at 90°C for 2 minutes. This gave a resist thickness of approximately 350nm. The dosage in our machine is 100 μC/cm^2.

Since our waveguides are about 1 cm in length, in order to eliminate stitching error in EBL, a technique called FBMS (Fixed Beam Moving Stage) is used. In this, the beam rotates about its mean position, while the stage is moved under it, exposing the patterned region.

The wafers are then developed in the developer maD-525 for 2 minutes.

Step 4: Ion milling to remove titanium from the non waveguiding region

Ion milling with argon ions is used to etch off the titanium from the remaining area.

Figure 9. Image of Ti layer after ion milling and washing

Step 5: Diffusion

Finally, the substrate is placed in an oven, and heated at 1000^{o}C for 10 hours, to completely diffuse the titanium into the substrate, forming the waveguiding region.

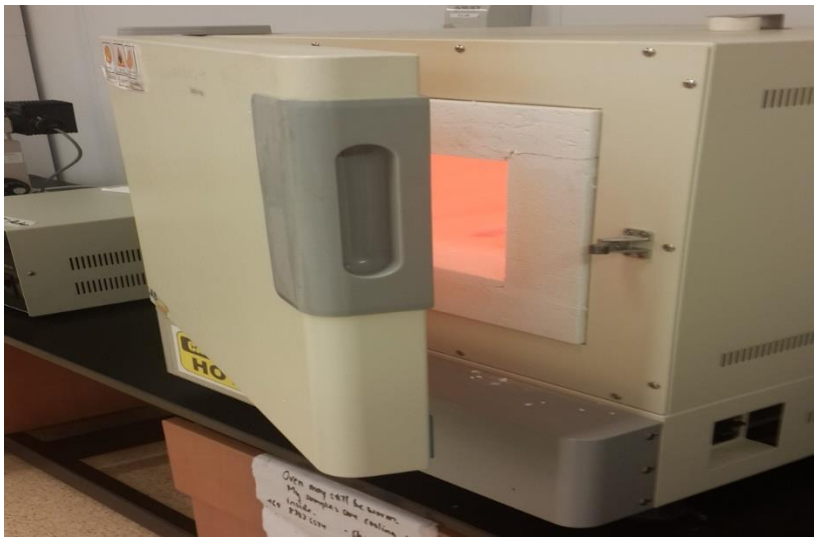

Figure 10. Experimental setup: Oven

2.2.3 Results

The index change in the waveguiding region made by titanium diffusion was measured using prism coupling. Details of the measurement are presented in Appendix C. The index change varied between 0.0025 to 0.005. After this, FSR measurements were performed on the large ring resonators fabricated.

Fig.12 (a) shows the schematic of the measurement set up. The transmission spectrum was measured using a broadband laser (SuperK Versa, NKT Photonics) with a wavelength range of 500nm to 1600nm.

The free space laser was focused using a 20x microscope objective onto the waveguide. The output was coupled into a lensed fiber and measured via an optical spectrum analyzer (Agilent 86142B OSA). The setup is shown in Fig.12 (b). The second set of measurements was performed to measure the FSR, which required significantly higher resolution as the FSR is expected to be 0.049nm, measured with an optical spectrum analyzer.

Large ring resonators were fabricated using the above described process. The rings, upon illumination with an Agilent 81980A tunable laser, showed an FSR of 0.049 nm.

The findings were presented in the OMN conference in 2014.

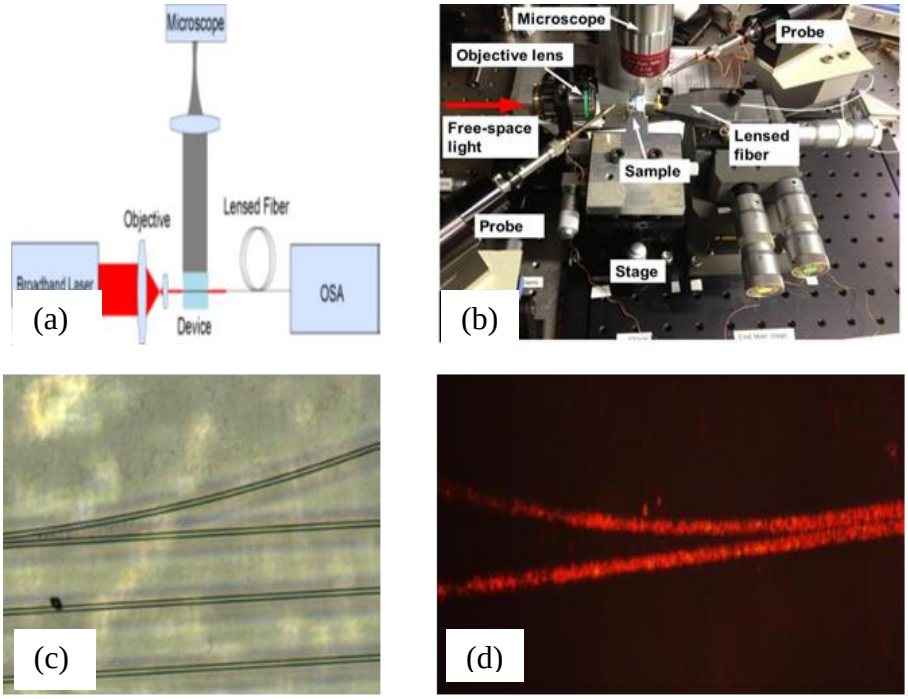

Figure 11. (a) Schematic of Setup; (b) Experimental setup for lensed coupling; (c) Ti diffused waveguides and racetrack resonator seen under an optical microscope; (d) The racetrack and the bus waveguide illuminated with a broadband laser centered at 1064nm.

2.2.4 Conclusion for Ti diffusion

The low index contrast of the Ti diffused waveguides were not suitable for the production of compact microphotonic structures, or high Q factor large ring resonators usable in microwave photonics experiments.

However, our trials with the titanium diffusion process, as it was the case with the proton exchange process, enabled us to optimize our fabrication parameters for e-beam metal deposition, photolithography, E-beam lithography, and ion milling; thus paving our pathway to the formation of devices on LNOI chips.

We also used the opportunity to organize our measurement setup, which was later used in the characterization of our rib and ridge devices on LNOI, as elaborated in the next section.

2.3 References

References for Proton Exchange:

[1] M. N. Armenise. “Fabrication techniques of lithium niobate waveguides.” IEEE Proceedings on Optoelectronics, vol. 135, pp. 85-91, (1988).

[2] R. W. Keys, A. Loni, and R. M. De La Rue, “Measurement of the increase in the SHG coefficient of proton exchanged LiNbO after annealing using a grating diffraction technique,” Electronics Letters, vol. 26, pp. 625–627, (1990).

[3] F. Laurell, M. G. Roelofs, and H. Hsiung, “Loss of optical nonlinearity in proton-exchanged LiNbO waveguides,” Applied Physics Letters, vol. 60, pp. 301–303, (1992).

[4] M. L. Bortz and M. M. Fejer, “Measurement of the second-order nonlinear susceptibility of proton-exchanged $LiNbO_3$,” Optics Letters, vol. 17, pp. 704–706, (1992).

[5] W.-Y. Hsu, C. S. Willand, V. Gopalan, and M. C. Gupta, “Effect of proton exchange on the nonlinear optical properties of $LiNbO_3$ and $LiTaO_3$,” Applied Physics Letters, vol. 61, pp. 2263–2265, (1992).

[6] T. Suhara, H. Tazaki, and H. Nishihara, “Measurements of the reduction in SHG coefficient in LiNbO by proton exchanging,” Electronics Letters vol. 25, pp. 1326–1328, (1989).

[7] X. Cao, R. Srivastava, R. V. Ramaswamy, and J. Natour, “Recovery of second-order optical nonlinearity in annealed proton-exchanged $LiNbO_3$,” IEEE Photonics Technology Letters, vol. 3, pp. 25–27, (1991).

[8] K. El Hadi, M. Sundheimer, P. Aschieri, P. Baldi, M. P. De Micheli, D. B. Ostrowsky, and F. Laurell, “Quasi-phase-matched parametric interactions in proton-exchanged lithium niobate waveguides,” Journal of Optical Society America B, vol. 14, pp. 3197–3203, (1997).

[9] J. Rams, J. Olivares, and J. M. Cabrera, “High-index proton-exchanged waveguides in Z-cut LiNbO with undegraded nonlinear optical coefficients,” Applied Physics Letters, vol. 70, pp. 2076–2078, (1997).

[10] Suchoski et. al. “Stable low-loss proton-exchanged $LiNbO_3$ waveguide devices with no electro-optic degradation.” Optics Letters, vol. 13, pp. 1050-1052, (1988).

[11] Raghuram Narayan. “Electrooptic Coefficient Variation in Proton Exchanged and Annealed Lithium Niobate Samples” IEEE Journal of Selected Topics in Quantum Electronics, vol. 3, No. 3, (1997).

References for Titanium Diffusion:

[1] J. A. Abernethy, "Novel devices in periodically poled lithium niobate," Doctoral Thesis, Faculty of Engineering and Applied Science, Optoelectronics Research Centre, University of Southampton, (2003).

[2] M. Fukuma and J. Noda, "Optical properties of titanium-diffused $LiNbO_3$ strip waveguides and their coupling-to-a-fiber characteristics," Applied Optics, vol. 19, pp. 591-597, (1980).

[3] J. X. Chen, T. Kawanishi, K. Higuma, S. Shinada, J. Hodiak, M. Izutsu, W. S. C. Chang, and P. K. L. Yu. "Tunable Lithium Niobate Waveguide Loop." IEEE Photonics Technology Letters, vol. 16, pp. 2090-2092, (2004).

[4] R. Keil, F. Auracher. "Coupling of single mode Ti-diffused LiNbO waveguides to single mode fibers." Optics communications, vol 30, pp 23-28. (1979)

[5] H. Hu, R. Ricken, W. Sohler. "Low-loss ridge waveguides on lithium niobate fabricated by local diffusion doping with titanium." Applied Physics B, vol. 98, pp. 677-679, (2010).

3. LITHIUM-NIOBATE-ON-INSULATOR

3.1 Introduction

The two most common techniques for photonic device fabrication on lithium niobate are titanium diffusion and proton exchange. However, due to very low refractive index contrast (usually less than 0.1), the waveguides formed through these processes have low mode confinement, high bending losses, and often, are not polarization independent, making it difficult to fabricate compact photonic structures on the material, as our investigation on the techniques showed.

Lithium-niobate-on-insulator (LNOI) provides a viable solution to the problem. This chapter describes the fabrication techniques we developed and optimized to produce low loss waveguides and resonators in LNOI. Lithium-niobate-on-insulator chips comprise a thin film of lithium niobate (thickness: ~700nm) adhering on an insulator substrate like SiO_2. Such devices provide good vertical and lateral index contrast and mode confinement. Also, because of the smaller waveguide widths attainable through etch based techniques, a greater control of the critical dimensions of devices is possible. We fabricated and characterized optical waveguides, power splitters, and microring resonators on LNOI chips, employing robust fabrication techniques, namely EBL and ion milling. The structures were characterized in terms of propagation loss and quality factor. The fabricated structures showed good performance, and the fabrication techniques have potential for use in the mass manufacture of lithium niobate based optical devices.

3.2 Structure of Lithium-niobate-on-insulator

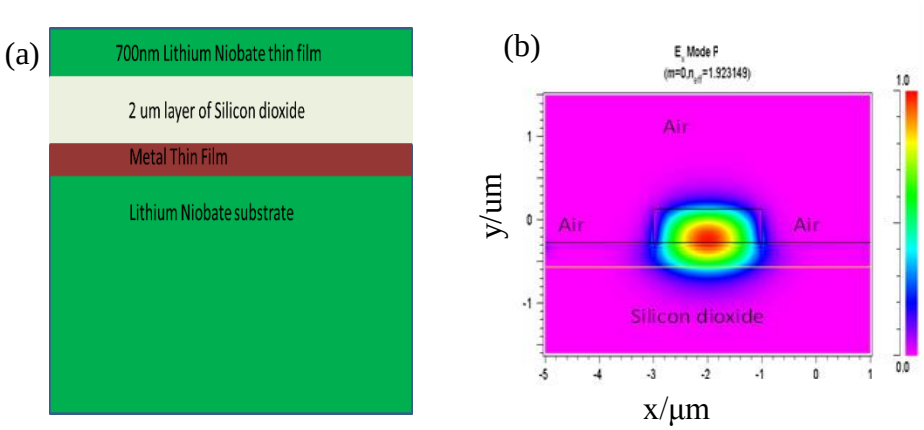

Figure 12. (a) Cross section of LNOI Chip; (b) TE mode profile in a rib waveguide on LNOI

LNOI chips are fabricated using ion implantation on bulk lithium niobate, followed by wafer bonding the thin layer to a layer of silicon dioxide [1]. For our experiments, we purchased the chips from NanoLN, Jinan Jingzheng Electronics Co., Ltd.

The schematic of the wafer is shown in Fig.13(a). The cross section comprises bulk lithium niobate on the bottom, an optional layer of platinum or gold, which can serve as an electrode, a layer of silicon dioxide on top of the metal, and finally a 700nm layer of lithium niobate thin film. The top layer is formed by ion implantation, and is subsequently wafer bonded to another lithium niobate wafer with a silicon dioxide layer on top. Crystal ion slicing is used to crack the top wafer at the implantation depth. Chemical mechanical polishing is used to thin the thin film layer to the desired thickness.

If a ridge or a rib waveguide is formed on the thin film, the mode is confined in three sides by air, and at the bottom by the silicon dioxide layer, as shown in 13(b). This enables the fabrication of ultra-compact devices on LNOI.

The height and width of the waveguides can be precisely controlled during fabrication, allowing the design of single mode waveguides, which are favorable for high speed data transfer. Thinner waveguides also result in higher electric fields, decreasing the working voltage, and allowing the possibility of fabricating MZI's that are one tenth the size of conventional, diffusion based MZIs. Furthermore, the waveguiding regions remain untouched, leaving their crystalline structure intact, resulting in higher Pockels coefficients and lower operating voltages than diffusion based MZIs.

Furthermore, the ion slicing techniques that are used to form LNOI chips have the potential to be used to bond microlayers of lithium niobate onto silicon chips, enabling the production of on chip MZI devices integrated with silicon photonics.

3.3 Etching Lithium Niobate

In order to fabricate ridge or rib waveguides, lithium niobate has to be etched first. However, lithium niobate is known for its etch resistivity. Inductively coupled plasma etching has been shown to be effective in the etching process, but produces waveguides with very rough sidewalls [2]. Wet etching with a mixture of fluoric, perchloric and acetic acids have been used in literature to produce waveguides, but it is difficult to get a vertical sidewall profile using the method [3]. A mixture of HF and HNO_3 can be used to etch ion implanted or proton exchanged lithium niobate, but generally, the etch rate is slow, difficult to control, and produces rough sidewalls [3]. Another technique is focused ion beam (FIB) milling, but the technique is not suitable for mass production or for the production of large, centimeter length structures [4]. Using metal masks,

reactive ion etching (RIE) has been used to fabricate waveguides with sidewall angles as high as 71 degrees [5].

Recently, freestanding high-Q-factor (100,000) microdisk resonators were demonstrated on LNOI, fabricated using RIE with argon ions [6].

We decided to employ the ion milling technique to fabricate our devices. We started by fabricating rib and ridge waveguides, which formed the building blocks of the subsequent structures.

Once the fabrication parameters for waveguides were optimized, splitters, directional couplers, and integrated microring and racetrack resonators were fabricated.

The following section describes all the fabrication steps in detail.

3.4 Fabrication of Devices

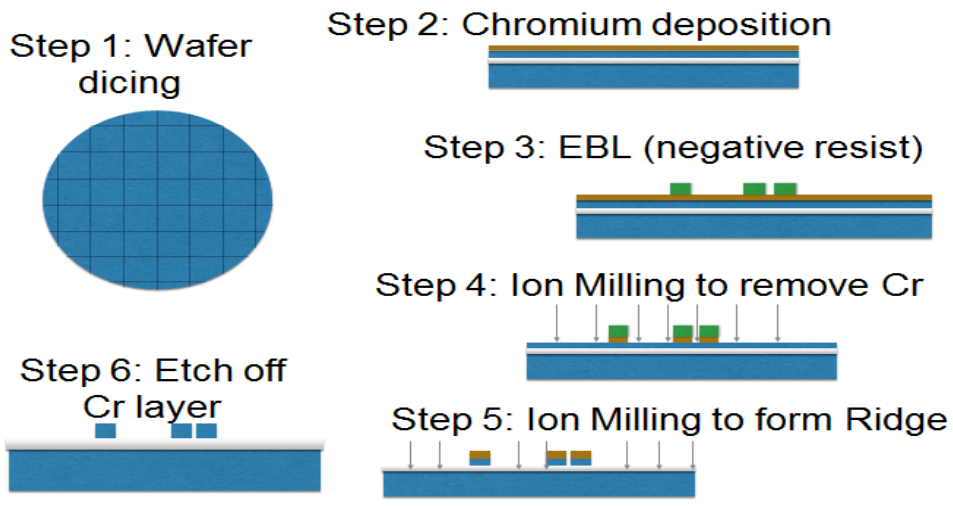

Figure 13. Fabrication of optical devices on LNOI

Fig. 14 shows the steps in the fabrication of optical devices on lithium-niobate-on-insulator chips. The steps are described below in further detail.

Step 1: Dicing

Since lithium niobate has hardness similar to glass, it is difficult to snap it into squares using a diamond cutter.

Using a commercial dicer, the wafer is first diced into 1cm by 1.2 cm blocks.

Step 2: Chromium deposition

Between each step, the sample is washed in an ultrasonic bath in acetone, isopropanol, and water respectively, for five minutes each. This is to ensure that the surface does not have any dust particles on it before the deposition.

Next, the substrate is covered with a 40-50nm layer of chromium, which acts as a conducting layer for EBL. The chromium is deposited using an electron beam evaporator. The layer has to be uniform so that the waveguides have the same height throughout the wafer after the etching.

The deposition is done in a vacuum of 6.0 E -6 Torr, at a rate of 0.1nm/sec, to ensure uniform deposition.

A surface profiler is used to check the final height of the layer after deposition.

Step 3: Electron Beam Lithography with negative resist

Fig. 19 shows the steps in EBL. A thin layer (30nm) of chromium is deposited on lithium niobate as a conductive layer.

We used ma-N 2403, a negative photoresist, to pattern our wafers. It is spin coated, with the speed ramped from 0 to 3000rpm at 1000rpm/s, then steady at 3000rpm for 30s, and finally ramped down at 1000rpm/s to 0rpm.

An EBL dosage of 120 μC/cm^2 is used to pattern the desired structure.

The resist is developed in ma-D 332 for 40 seconds.

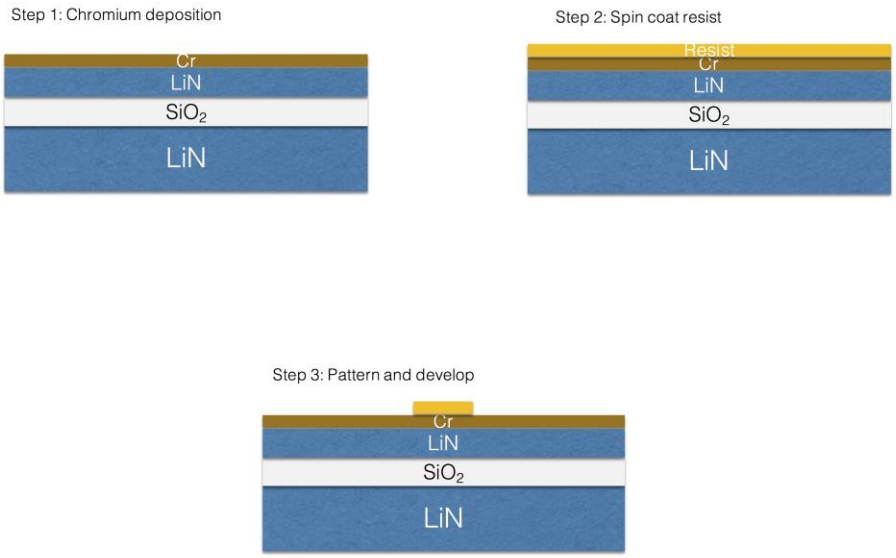

Figure 14. Steps in Electron Beam Lithography

Steps 4 and 5: Ion milling to remove chromium and lithium niobate

Ion milling with argon ions is used to etch off the chromium and the lithium niobate, forming 300nm ribs.

Chromium and lithium niobate have similar etch rates ~15nm/min, when ion beam current of 110mA, beam voltage of 300V, RF power of 170W and an angle of 90° to the substrate. A 23 minute etch is sufficient to etch off around 50nm of chromium and form 300nm ribs.

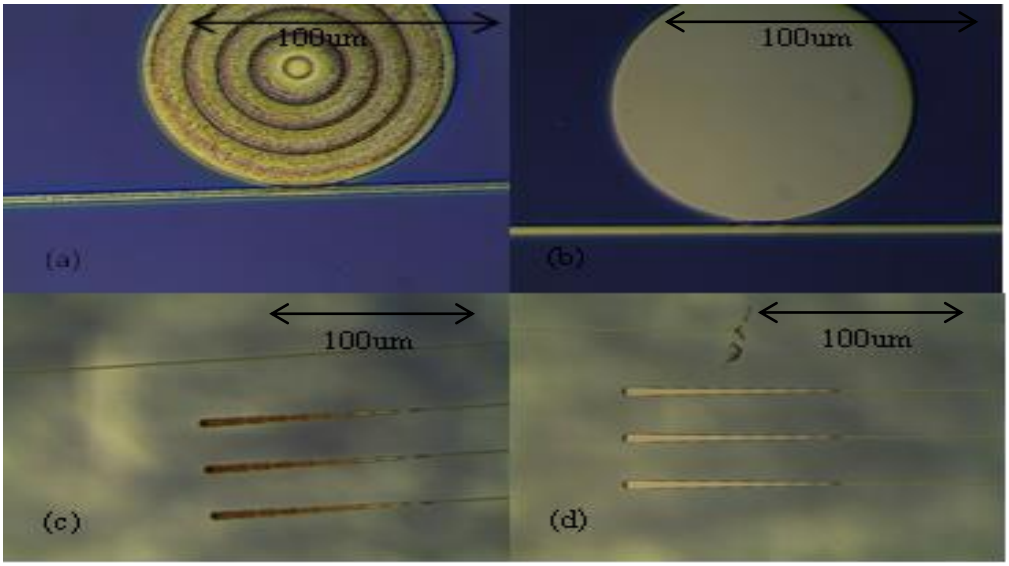

Figure 15. (a) Microdisk resonator before ozone stripping; (b) Microdisk resonator after ozone stripping: (c) Tapers before ozone stripping; (d) Tapers after ozone stripping

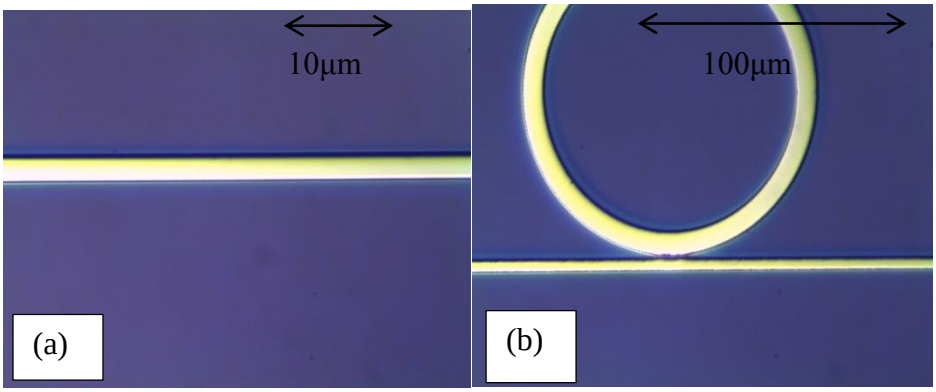

Figure 16. (a) Rib waveguide after ozone stripping; (b) Microring resonator and bus waveguide after ozone stripping

Step 6: Stripping off the remaining resist and chromium

The exposed photoresist is washed off by acetone. Ozone stripping is done for 15 minutes at 100^{o}C to strip of any remaining resist. The chromium is washed off by wet etching. The samples are subsequently diced to get optically smooth end facets to facilitate the coupling of light into the waveguides.

3.5 Optimization of Process Parameters

3.5.1 Dicing

First, the wafer needs to be diced in ordered to divide it into 1cm by 1.2 cm segments. Our devices are typically 1cm in length. For LNOI, we get the wafers pre-diced into our required sizes.

Because lithium niobate has hardness similar to glass, it is not feasible to crack it using a diamond cutter like a silicon wafer.

After waveguide fabrication, we diced the wafer using a commercial Disco dicer. The wafers are 0.5 mm thick. The back end of the wafer was cut to form a groove of 0.4 mm. The remaining portion is cracked, to give the surface an optically smooth end facet.

A high rotational speed of the blade (20000rpm) and a low feed speed (1mm/s) produces the best cuts.

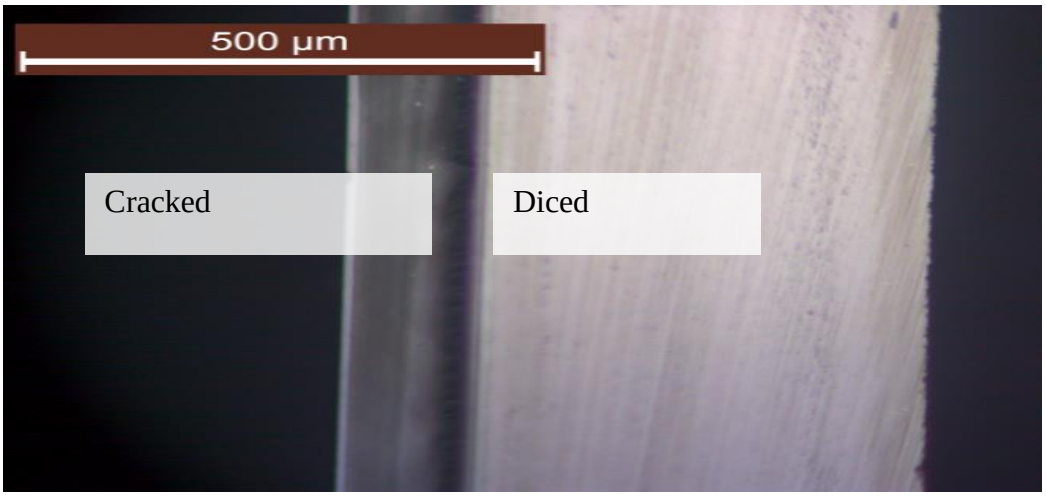

Figure 17. Cross section of a wafer after dicing and cracking. The cracked portion is optically smooth.

3.5.2 Electron beam lithography

Our goal is to make waveguides with thicknesses ranging from 1 micron to 10 microns, and resonators ranging from a few microns to a few centimeters in diameter. In order for the waveguides to couple light into the resonators, the gap between the resonators and the waveguides must be in the order of a hundred nanometers.

The etch rate for ma-N 2403 and lithium niobate is about 1:1.

Since our waveguides are about 1 cm in length, in order to minimize the stitching error, a technique called FBMS (Fixed Beam Moving Stage) is used.

In direct writing, the beam traverses the pattern area from one end to other, filling the write-fields one by one. For long patterns, some of the write-fields can get misaligned, ruining the whole pattern.

In FBMS, the beam rotates about its mean position, while the stage is moved under it, exposing the patterned region. As a result, there are no write-fields that require to be stitched, and stitching error is eliminated. The speed of the stage and the beam dosage had to be optimized before waveguides with acceptable performances were obtained.

The top of some waveguides retained marks of the FBMS path, as shown in Fig. 19 (a). Furthermore, in some of the waveguides, the sidewalls showed a wavy feature, that was caused by the non-overlapping electron beam exposures of the resist in the FBMS path.

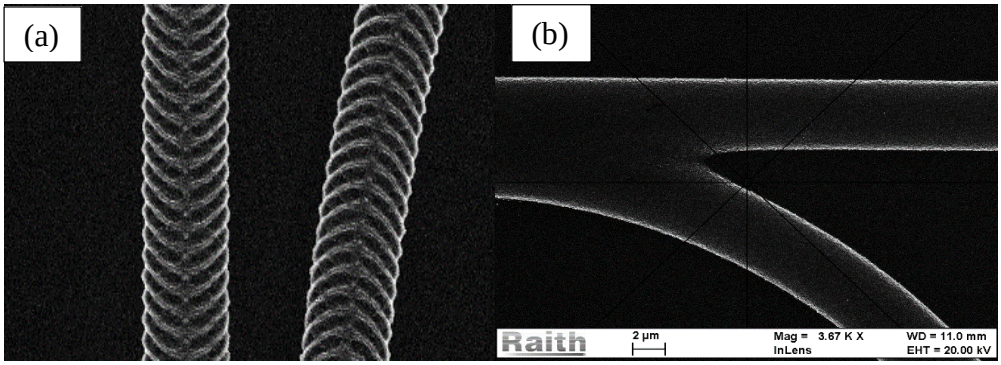

Figure 18. (a) SEM showing typical profile of resist after pattering at a high FBMS speed; (b) SEM showing resist patterned at a slow FBMS Speed

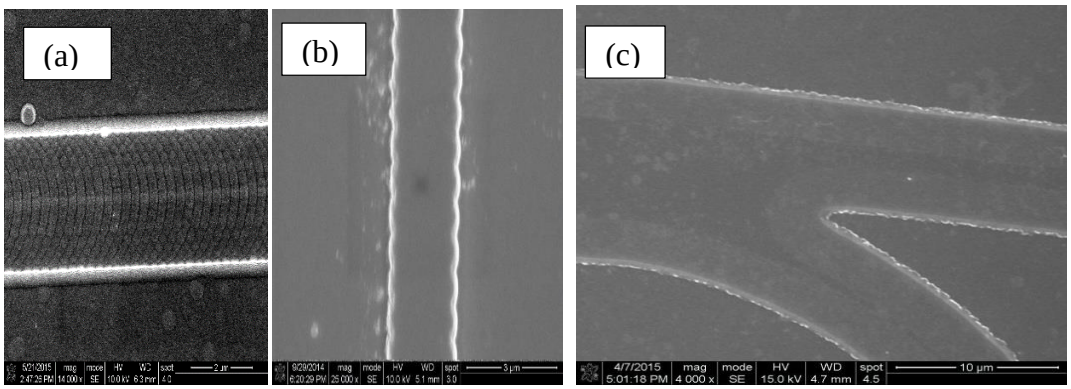

Figure 19.(a) Waveguide profile after ion milling a pattern with a higher FBMS speed, showing irregularities on top surface; (b) 'Wavy' sidewalls produced after etching; (c) SEM of waveguide patterned at a slower FBMS speed.

The roughness, as measured by an AFM, has RMS values over 40 nm. The roughness scatters light, causing the propagation loss in our first waveguides to be as high as 30dB/cm at a wavelength of 1550nm.

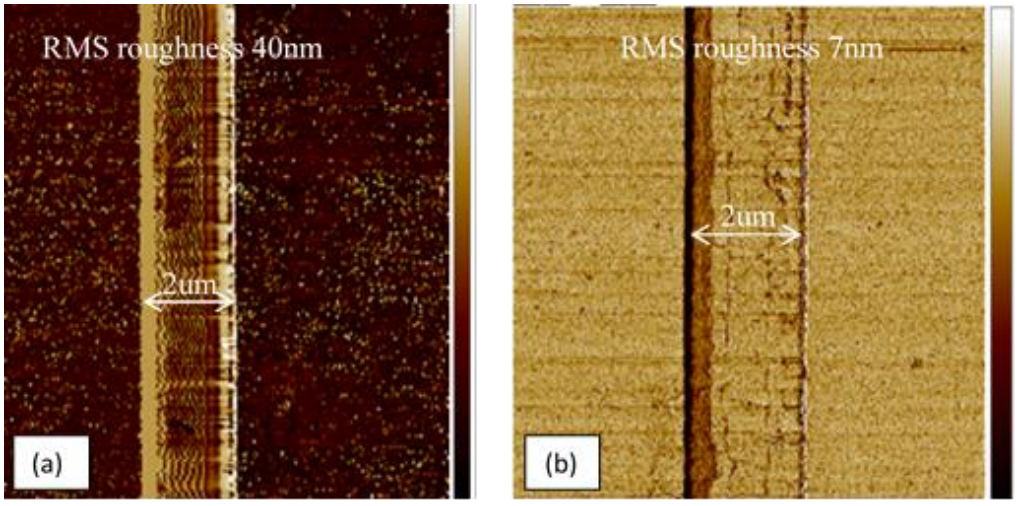

Figure 20. (a) AFM image of waveguides with surface irregularities; (b) AFM of waveguides with better smoother surfaces.

Other than using a lower FBMS speed, other techniques can be used to counter this problem.

The first method is double patterning. As seen Fig. 22, the portion of a Y-branch splitter that got a double dose of e-beam because of overlapping FBMS beam paths, has a smoother profile after etching.

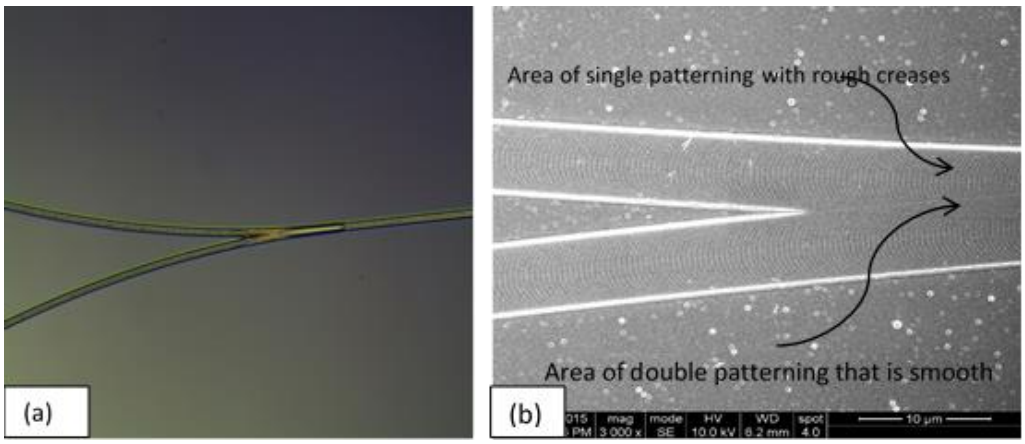

Figure 21. (a)Optical microscope, and (b) SEM image of a splitter, showing a smoother profile where double patterning took place.

To pattern my waveguides and ring resonators, I used the double patterning scheme, where the electron beam swipes each area two times, thus evening out the dosage. This resulted in the smooth top surface for the waveguides. A post exposure bake to reflow the resist also helped take out the roughness from the top.

The best results were obtained by doubly exposing the resist, followed by a post bake reflow.

The waveguides are developed using maD-332 for 45 seconds. A post-exposure bake of 120^{o} C for five minutes is done, before they are ion milled. The post-exposure bake hardens the resist to improve etching resistance.

3.5.3 Techniques to reduce the sidewall roughness

In the initial recipe, the devices were ion milled for a total time of 18 minutes, broken down into six segments of 3 minutes, alternating the ion milling angle between 90^{o}, to give higher etch rate, and 70^{o}, to remove any redeposited layer.

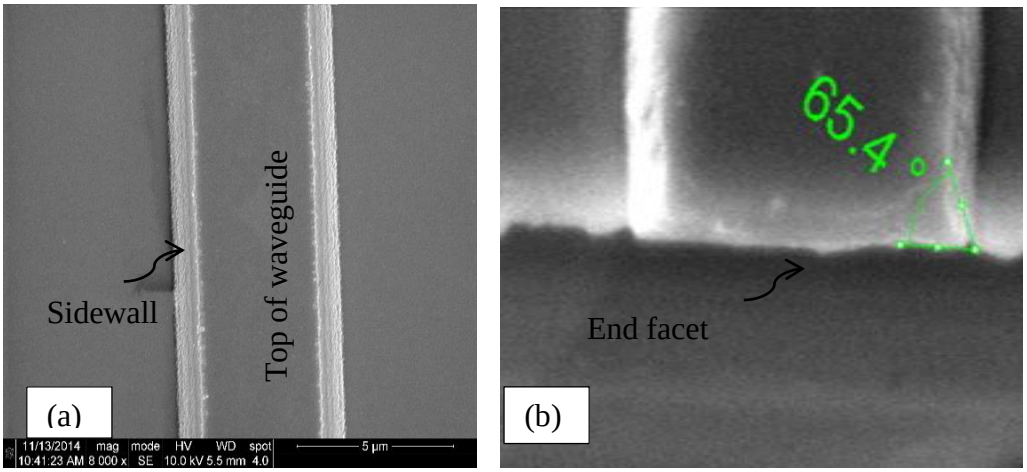

Figure 22. SEM showing (a) rough sidewalls of 4µm waveguides; (b) Sidewall angle after etching

However, the resulting waveguide profile was as follows.

As for the sidewall angle, it is possible to get more vertical sidewalls using a thicker (~1µm) layer of resist. However, a thicker layer makes it more difficult to pattern the ~100nm gaps for light to couple from our bus waveguides to the ring resonators. At this point, we focused more on the sidewall roughness of the waveguide, because it was contributing to propagation loss.

The grains on the sidewalls are a result of redeposited lithium niobate. Upon close inspection, it was seen that in addition to the grainy redeposition, there were six distinct layers visible in the sidewalls, attributed to the six etch steps. This showed that our initial etching strategy had failed to produce smooth sidewalls. Sidewall roughness has a significant contribution to the loss in waveguides.

To get smooth sidewalls, several techniques were tried out.

3.5.4 **Annealing**

Wang et al had demonstrated high Q-factor disk resonators formed by annealing suspended microdisks beyond their curie temperature [7]. In our previous experiments involving rib structures in bulk lithium niobate, it was seen that annealing devices past the Curie temperature resulted in smooth sidewall profiles in bulk lithium niobate, as shown in Fig. 24(c) and (d).

However, annealing at such high temperatures caused the LNOI samples to crack and completely destroyed any pattered devices. A reason for this could be that silicon dioxide and lithium niobate expand at different rates at high temperatures. The resultant stress destroys the thin layer of lithium niobate on the silicon dioxide.

Nevertheless, annealing for long hours (10-12 hours) at lower temperatures (450^{O}C) was tried out to see if they had any effect on the sidewalls. The results were negative, and the sidewall profiles were the same as before.

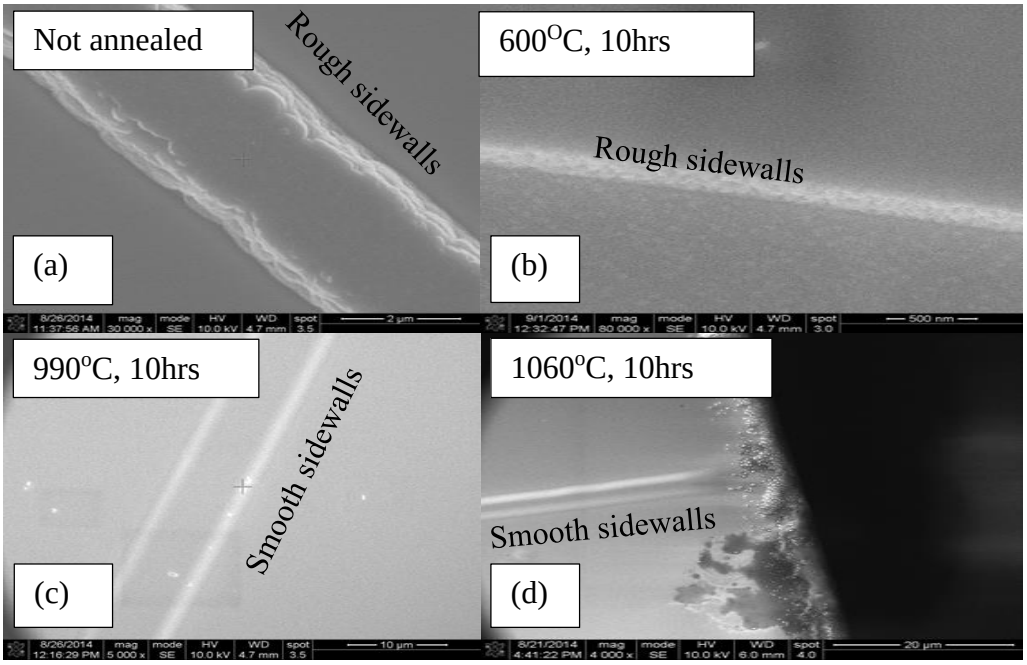

Figure 23. (a) Typical rough sidewalls in a waveguide, post ion milling; (b) Rough sidewalls of a waveguide after low temperature annealing; (c) and (d) Smooth sidewalls obtained by annealing at high temperatures.

3.5.5 **Wet etching**

The next technique tried out to get smooth sidewalls was wet etching. 45% concentrated hydrofluoric acid was used to etch off the irregular sidewalls. The etch rate for lithium niobate is 2-3 nm per minute. Ideally, a 20 minute etch was expected to attack the uneven sidewalls and dissolve away the granularities, which have a higher surface area than the smoother regions.

However, the etching by concentrated HF was seen to be highly uneven, and formed bubble like aberrations on the sidewalls. The etched off lithium niobate redeposited all around the substrate, and was impossible to remove with a standard acetone wash.

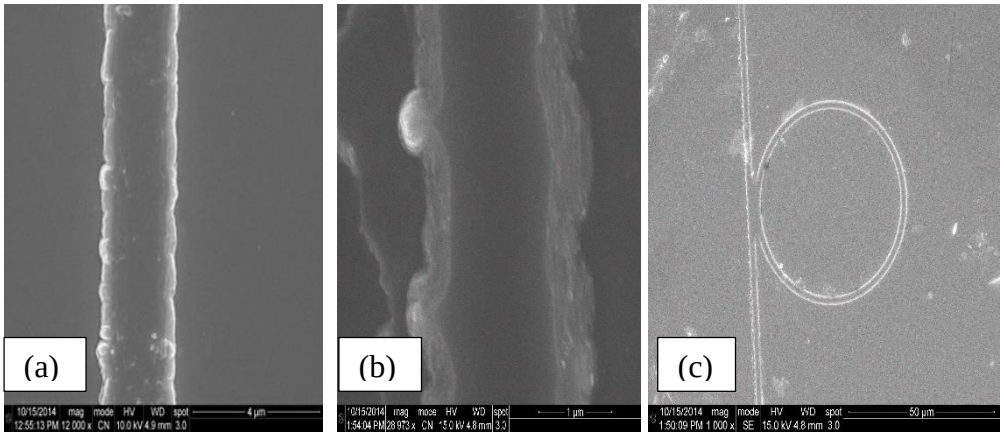

Figure 24. (a) SEM of waveguide after etching with HF; (b) Bubble like aberrations formed on the sidewall due to uneven etching; (c) Redeposition after HF over the substrate

Furthermore, HF was seen to attack the –Z side more than the +Z side, as supported by literature. This makes it unsuitable for use in the etching of Y propagating waveguides on X cut surfaces, and also for ring structures.

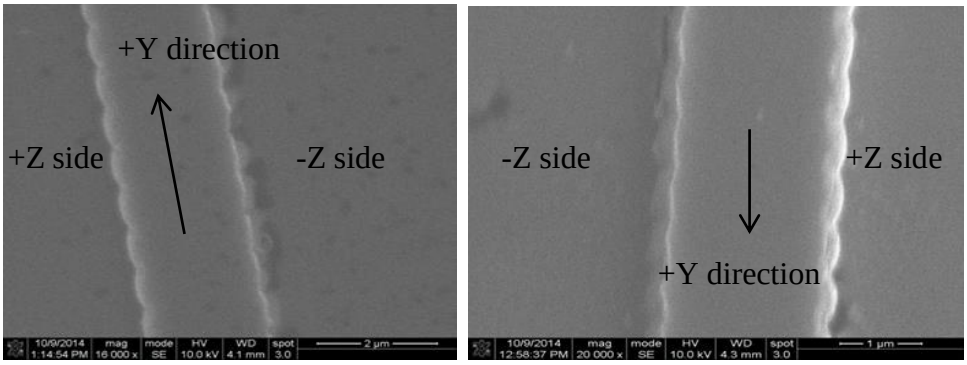

Figure 25. X cut, Y propagating waveguides showing uneven HF etch on +Z and -Z side

Possible solutions to the wet etching problem might be to sonicate the wafers in concentrate HF solution, to make the etching more uniform, and prevent the formation of bubbles. However, concentrated solution of hydrofluoric acid being very dangerous to work with, other solutions were implemented that did not require the usage of the acid.

3.5.6 Etching through

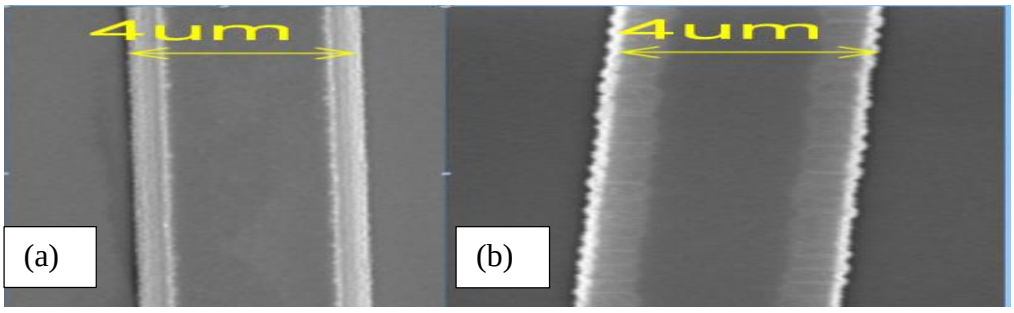

Figure 26. (a) A 4µm rib waveguide with rough sidewalls; (b) A 4µm wide ridge waveguide formed by etching down $LiNbO_3$ to the SiO_2 layer.

It was seen in literature [6] that free standing disks fabricated by ion milling on lithium niobate had smooth sidewalls. It was hypothesized that the roughness was called by self-sputtering of lithium niobate on the sidewalls during the etch process. Hence, etching down the lithium niobate to the silicon dioxide layer underneath seemed like a viable solution, to prevent the redeposition of lithium

niobate onto the sidewalls. For freestanding waveguides and rings, this technique did get rid of the redeposited particulates.

However, for structures placed closely together, this technique did not work. Self-sputtering occurred from one branch of the Y-branch splitter to the other, causing closely placed sidewalls to be rough. While this technique would work for devices made in isolation, this would not work for a Y-branch splitter, power couplers, or for a waveguide to ring coupler.

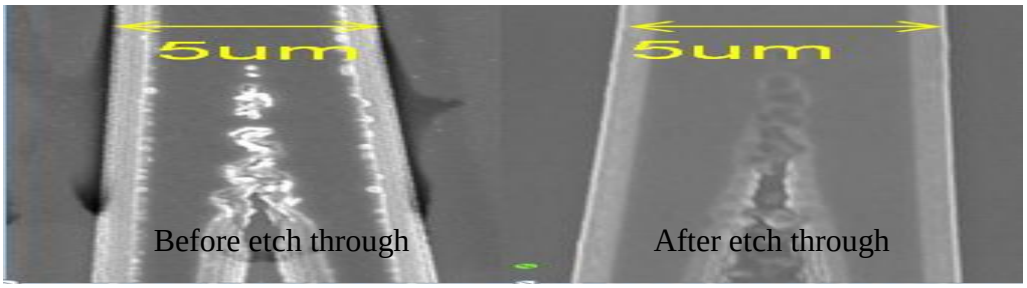

Figure 27. After etch through, the sidewalls smoothen out at the outer walls, but near the fork, there is still significant redeposition

3.5.7 Physical etching at a 45º angle

To etch away redeposited $LiNbO_3$, ion milling of samples were done at different milling angles, as showed in Fig. 29. Ion beam angles (θ) were varied from 90 to 45 degrees, at 15 degree steps. The redeposition on the sidewalls seemed to decrease as the angle got closer to 45 degrees.

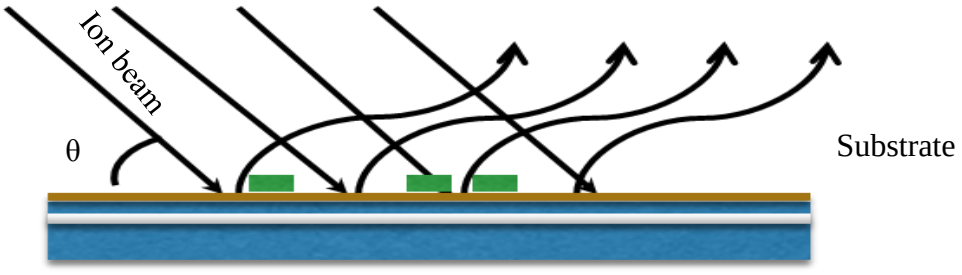

Figure 28. Optimization of ion milling angle

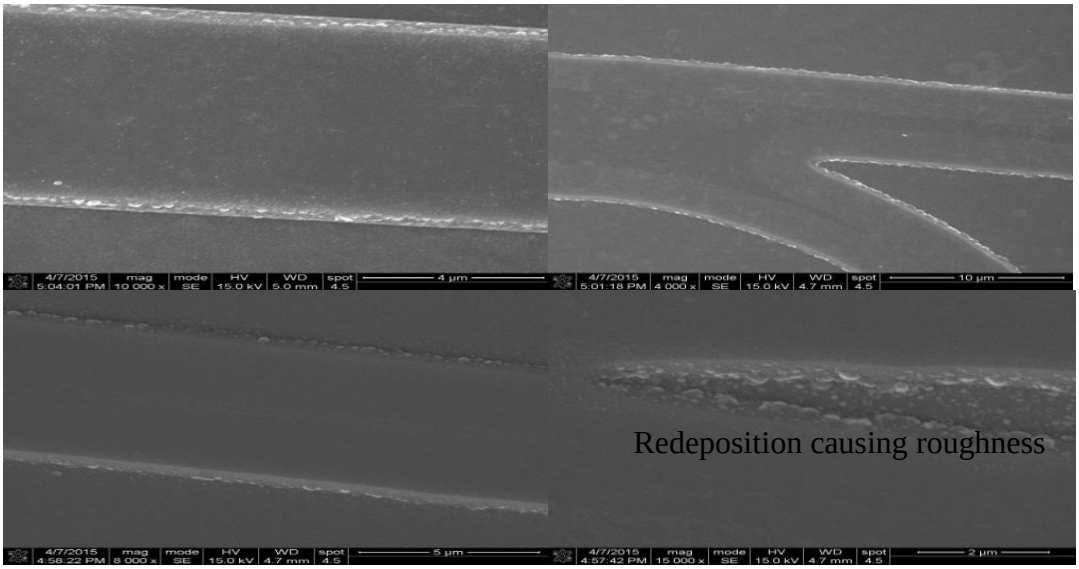

Figure 29. Waveguides and Y branches milled at 60º angles, showing a significant amount of redeposition near the branching and the sidewalls.

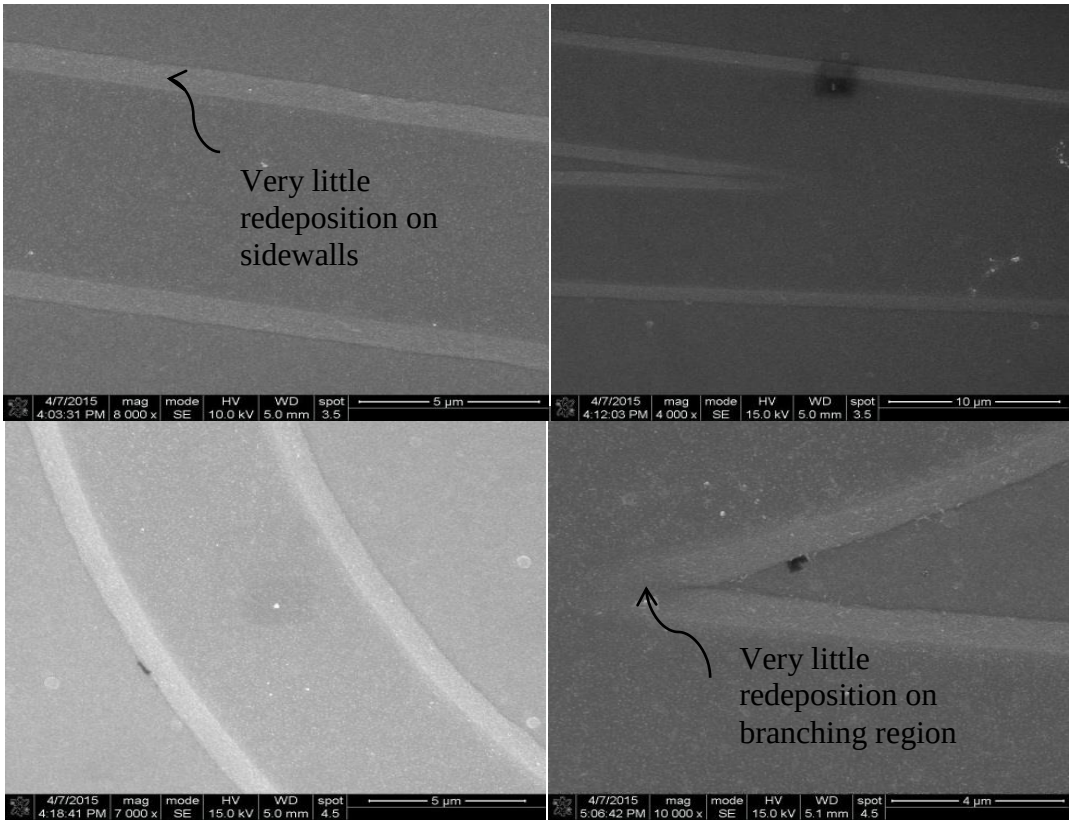

Figure 30. Waveguides, ring, and Y-branches milled at 45º angle, showing almost no redeposition even at the branching regions.

Ion milling at 45º gave the required smooth sidewall profile for isolated waveguides as well as closely placed structures. As the ion milling angle decreased however, the resulting sidewalls we obtained were less vertical.

3.6 Characterization of Devices

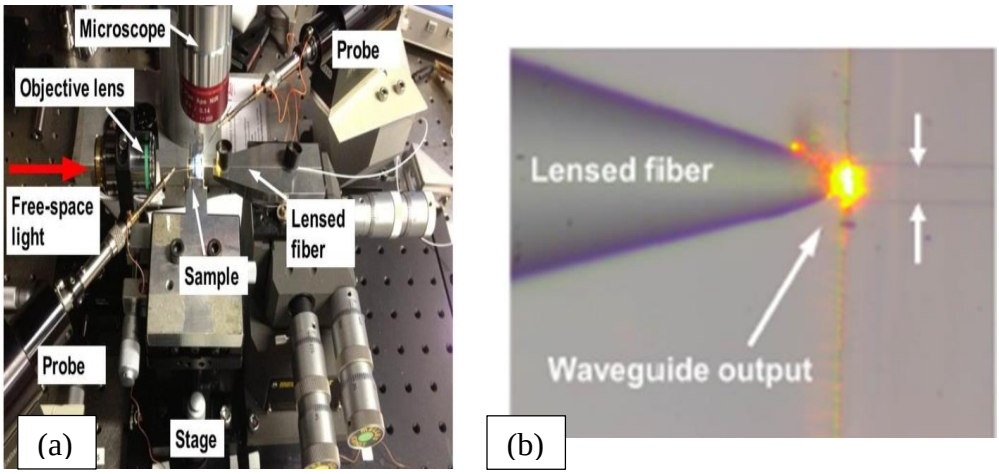

Figure 31. (a) Measurement set up with an objective lens used to focus laser at input; (b) A lensed fiber can be used to collect the light from the output of the waveguide

Fig.32 (a) shows the measurement set up we used to test out if our samples were coupling light. A lens (or a lensed fiber) is used to couple light into the waveguide. The wafer is mounted under an optical microscope, which can be used to align the laser to the waveguides, and also for the collection of light scattered from the sidewalls. Fig.33 shows some lossy samples illuminated with a supercontinuum laser centered at 1064 nm, with a wavelength range of 500 nm to 1600 nm. From the output, a multimode fiber collects the light and leads it to an optical spectrum analyzer.

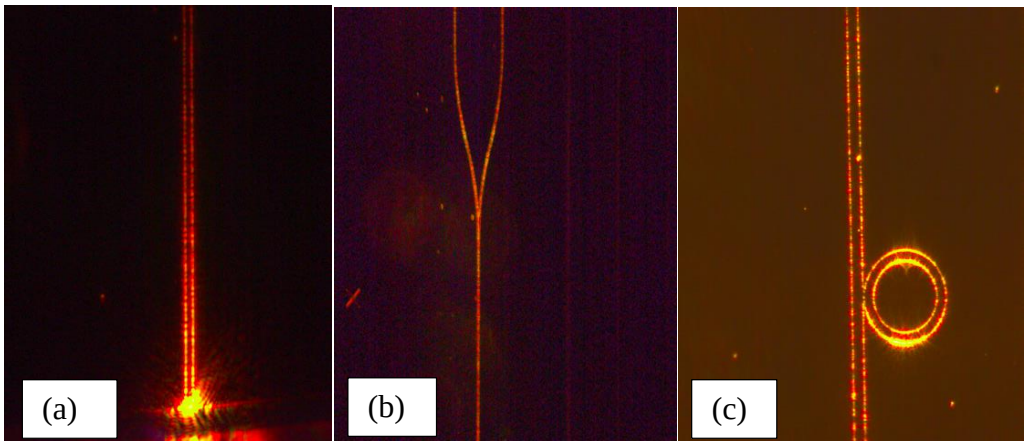

Figure 32. Images of (a) a lossy waveguide; (b) A lossy Y-branch splitter; and (c) A lossy ring resonator and a bus waveguide

3.6.1 **Waveguides**

Before we could move on to designing complex photonic structures, we started by optimizing fabrication parameters for waveguides.

Waveguides fabricated at the beginning of our project that had a rough top surface had losses over 10 dB/cm. In fig. 34(a), these can be seen to light up throughout the waveguiding region.

Fig. 34 illustrates a few illuminated waveguides at the initial stages of our project. The waveguides are 4 microns in width, and 300nm in rib height. Light at 1550nm is coupled into the waveguide using a tapered fiber. The waveguide is viewed from the top using an infrared camera. The images were taken with an integration time of 200 μs, using a 20x magnification objective lens. Because of the scattering from the rough surfaces, the waveguides light up when light is coupled into them.

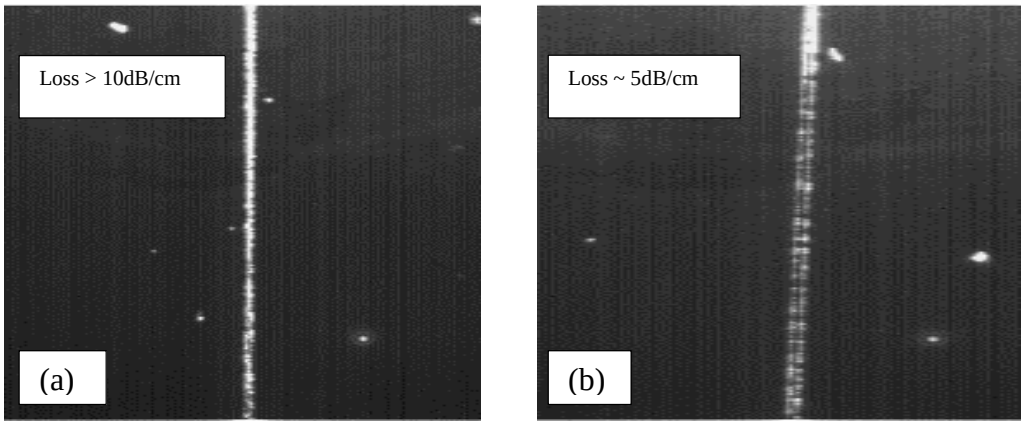

Figure 33. (a) Waveguide with a rough top surface; (b) Waveguide with rough sidewalls

The next figure shows a 4μm wide 300nm rib waveguide. Upon coupling, due to the smoothness of the sidewalls, there is little or no scattering of light as it travels through the waveguide. Hence, only the ends of the waveguides light up.

After the FBMS parameters were optimized, the loss reduced to 5 dB/cm, with most of the scattering occurring only at the sidewalls. This can be seen in Fig. 34(b), where, in contrast with (a), only the sidewalls of the waveguides light up. Our most recent results, where the waveguides are fabricated with a slow FBMS speed, double patterning, and angled ion milling, show losses less than 5 dB/cm. The waveguides, even when guiding light, are invisible under the microscope. Fig. 35 shows such a waveguide. The waveguide is visible only when an illuminator is used to shine light on the wafer. With the illumination turned off, only the spot at the output is visible.

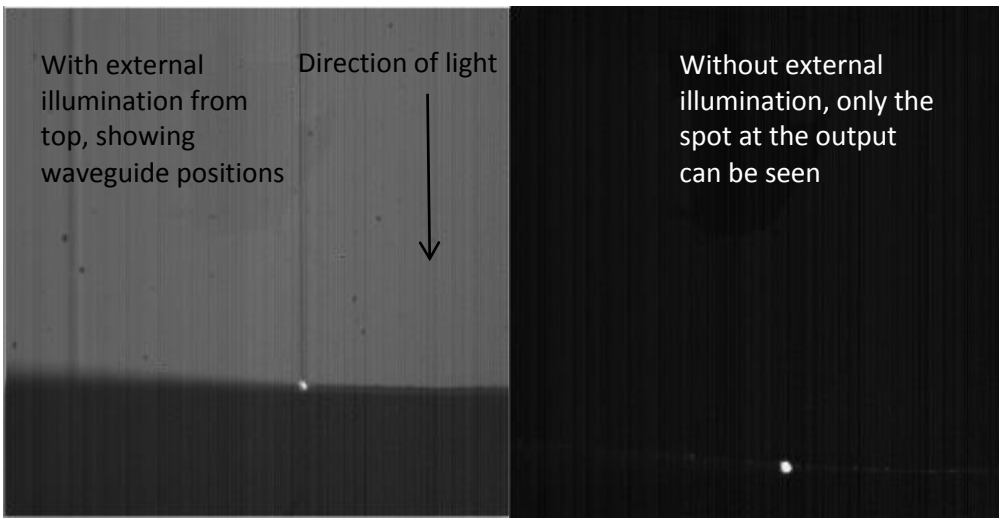

Figure 34. Waveguides after optimizing EBL and ion milling parameters

3.6.2 Loss measurement

For very lossy waveguides, the devices can be seen to light up when illuminated by a laser at a wavelength of 1550nm. The predominant mode of loss here is scattering. The following technique is used to measure loss [8, 9].

A snapshot of the waveguide is taken using an infrared microscope.

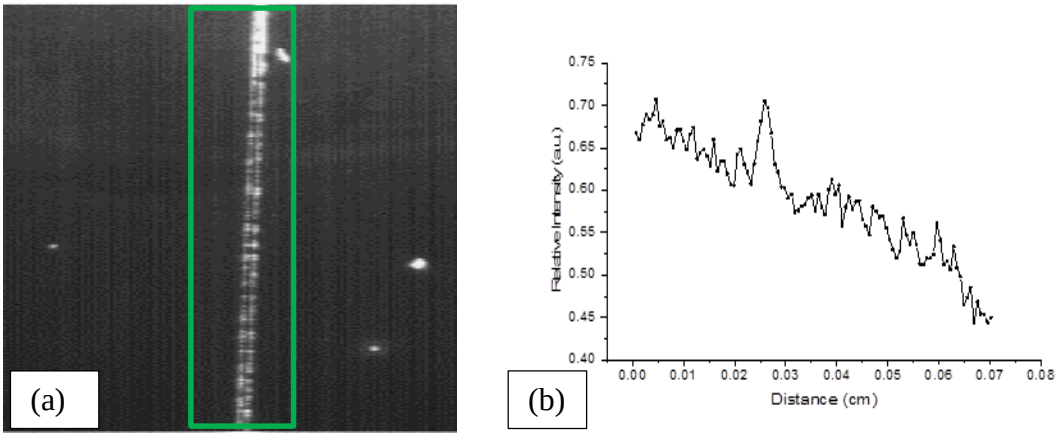

Figure 35. (a) Portion of image taken for processing; (b) Graph showing intensity vs distance

The image is then analyzed using an image processing software, and the pixels are given a numeric value (brighter pixels get a higher value, and so on).

Over the region of the waveguide, the brightness values are averaged, and a graph of brightness against distance is plotted.

From the best fit line, the loss can be calculated.

Once smooth sidewalls were achieved, there was no scattered light from the sides of the waveguides; hence, the waveguides could not be seen to light up under an optical microscope. Hence, the aforementioned technique could not be used to calculate the losses.

An alternative technique was developed to provide a rough estimate of the loss. Previously, we had designed Y-branch splitters showing a 50-50 power ratio in either arm. We fabricated Y-branch splitters with arms of different lengths. The

left arm has a length of 1mm from the branch, and the right one has a length of 2.5 mm. The 1.5mm distance is just enough so that both of the spots can be imaged in a single snapshot.

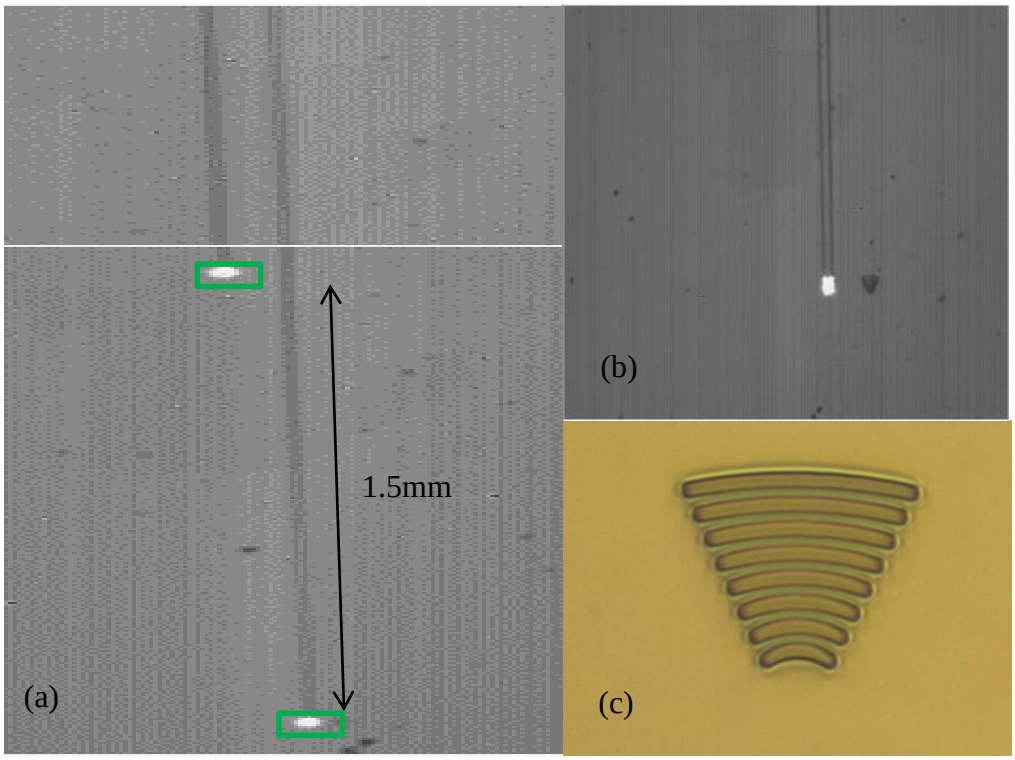

Figure 36. (a) Two snapshots showing two branches of the Y-branch splitter; (b) Lit up diffraction grating (lit) and freestanding diffraction grating (unlit); (c) The diffraction grating

A Y-branch splitter was used to divide the incoming beam of light into two equal parts. The branches are of uneven length, with one branch being 1.5mm longer than the other.

Diffraction gratings are placed at the end of the waveguides that scatter light upwards. The intensity of the light is measured by the optical microscope.

It was seen that structures horizontal to the laser direction have the tendency to scatter light, thus lighting up even when no light actually enters the waveguide. To make sure that the diffraction gratings were actually diffracting light that is coupled into the waveguide, and not uncoupled light escaping from the fiber, an additional freestanding diffraction grating was patterned beside the waveguide.

Only the grating that was directly aligned with the waveguide is lit up, showing that the diffracted light indeed came from the waveguide, and from stray, uncoupled light.

Using an Image processing software, numeric values were assigned to the pixels enclosed by the green boxes in Fig. 37 (a).

Now if the intensity of the grating at the smaller branch is I1, and that at the longer branch is I2, the estimated loss can be obtained from the power ratio.

Loss = 10 log (I1/I2) = 0.15 dB/cm. (Equation 2)

Readings were taken across several samples, and varied between 0.5 – 3 DB/CM. However, it should be noted that because the spots are actually different distances from the objective lens used to collect the light, factors such as chromatic and spatial aberration of the lenses, etc. can affect the value of measured loss.

However, it is clear from the images that the losses are far lower than that in our previously formed waveguides (<5dB).

Further work in this section might involve the setting up of a better loss measurement setup.

Two alternative methods for loss measurement are the cut-back method and the Fabry-Perot method.

In the cut-back method [10], the intensity of light at the end of the waveguide is measured using a tapered fiber at a particular distance, followed by dicing the wafer a set distance away from the previous facet. The light at the output facet is measured again at the new distance. The ratio between the light intensities at the output facets divided by the distance is the propagation loss. The process is repeated several times to get an average value of the propagation loss.

A non-destructive method to measure the loss in low finesse waveguides is the Fabry-Perot method [11], where the waveguide is treated as a resonator, and the end facet reflectivity and the propagation loss are extracted from the transmission spectra of the waveguides.

Either of the methods would provide an added avenue for measuring the loss of the rib waveguides more accurately.

At this point of our experiments, however, since one of our long term projects involved the fabrication of an ultra-compact MZI, the losses were deemed acceptable, and we moved on to working on our splitter and ring resonator designs.

3.6.3 3dB couplers and Y-branch splitters

This part of the project was done simultaneously with the optimization of waveguide losses.

Y branch splitters [12] 3dB couplers [13] are essential in the design of a wide array of integrated optical devices, like modulators, resonators, and switches. For our project involving the fabrication of MZIs, we simulated and designed some 3dB couplers and fabricated them on the LNOI samples.

The simulated couplers were made of 2μm wide, 300nm high rib waveguides, and had a coupling length of 330μm at a wavelength of 630nm.

The fabricated devices show close matches to the simulations.

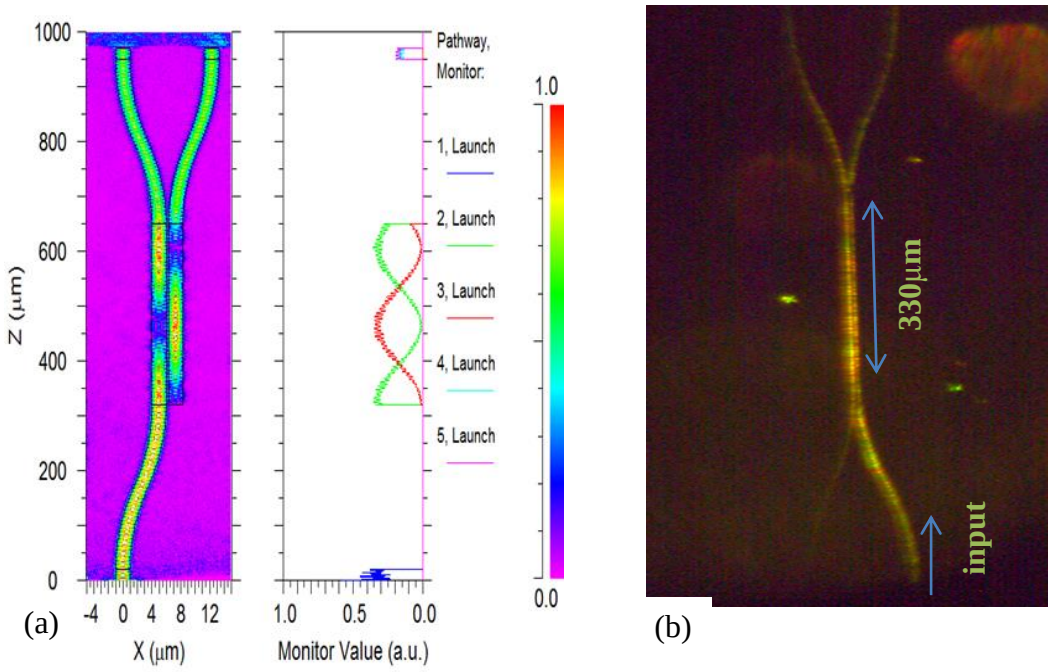

Figure 37. (a) BeamPROP simulation of 4μm wide 300nm rib 3dB coupler; (b) Optical image of an illuminated 3dB directional coupler.

However, simulations showed that directional couplers small (10%) changes in the gap between the waveguides would cause large changes in the power splitting ratio. Hence, for MZI fabrication, it would be a better idea to use Y-branch splitters, whose performance is more tolerant to fabrication errors.

Y-branch splitters were also designed using 2µm wide, 300nm deep rib waveguides. They show even power splitting, with less than 2% power difference between the left and the right arm. These were later used in the estimation of waveguide losses.

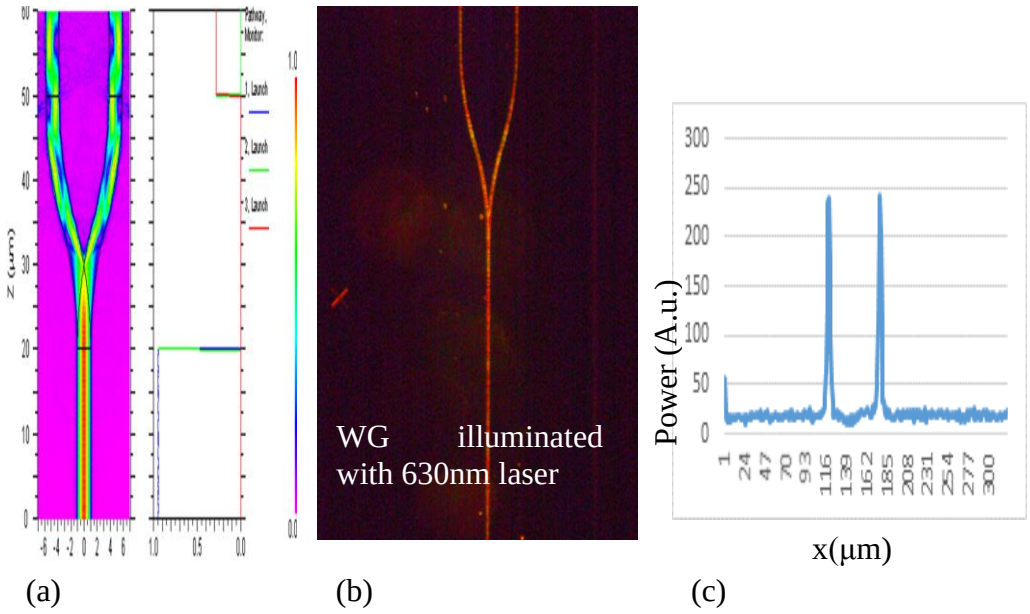

Figure 38. (a) BeamPROP simulation of Y-branch splitter; (b) A Y-branch splitter illuminated with light at 630nm; (c) Power in left and right arm.

3.6.4 Ring resonators

Ring resonators are particularly useful devices due to their small size and wavelength selectivity. They are able to provide many photonic functions such as optical delay lines, add-drop filters [12] and photonic sensors [16]. While fairly common in other materials such as silicon [16], polymer [17], and GaAs [18], microring resonators in LN are more difficult to fabricate due to the difficulty of working with LN.

Because of the fabrication difficulties associated with lithium niobate, however, few ring resonators have been realized in lithium niobate ($LiNbO_3$). Microring resonators in lithium niobate allow direct electrical control, leading to an ultrafast modulation response. Additionally, large, millimeter scale $LiNbO_3$ resonators can be used in mm-wave modulation with simultaneous RF and optical resonances [17, 18].

After achieving smooth sidewalls, we designed microring resonators on lithium-niobate-on-insulator chips.

We started by designing microring resonators with an external diameter of 108μm, and a waveguide width of 4μm.

The Free Spectral Range (FSR) of such a device is given by the following equation:

$FSR = \lambda^2/nl$ (Equation 3),

Where λ is the wavelength of the injected light, n is the refractive index of lithium niobate, and L is the length of the resonator.

The FSR for the microrings is calculated to be 3.25nm, at a wavelength of 1530nm. The experimental FSR was 2.92nm, which is slightly lower that the calculated FSR. An explanation could be a slight increase of the lithium niobate

crystal after ion implantation [19]. This is a matter that requires further investigation.

In order for our monolithic, microwave-optical modulators to work, large ring resonators with very small FSRs, comparable to microwave frequencies to be made. Modulation can only be observed if the microwave frequencies match the FSRs and resonance peaks.

1.55-millimeter-long racetrack resonators were designed, with coupling lengths of 187μm, and half circle radius of 187μm. The following diagram shows the image of a typical coupling setup. A single mode tapered fiber is used to shine infra-red light at the input end. The calculated FSR is 0.70nm. The measured FSR is 0.66nm, which is slightly lower than the measured FSR. This can be caused by a lowering of the refractive index of the lithium niobate substrate subsequent to ion implantation.

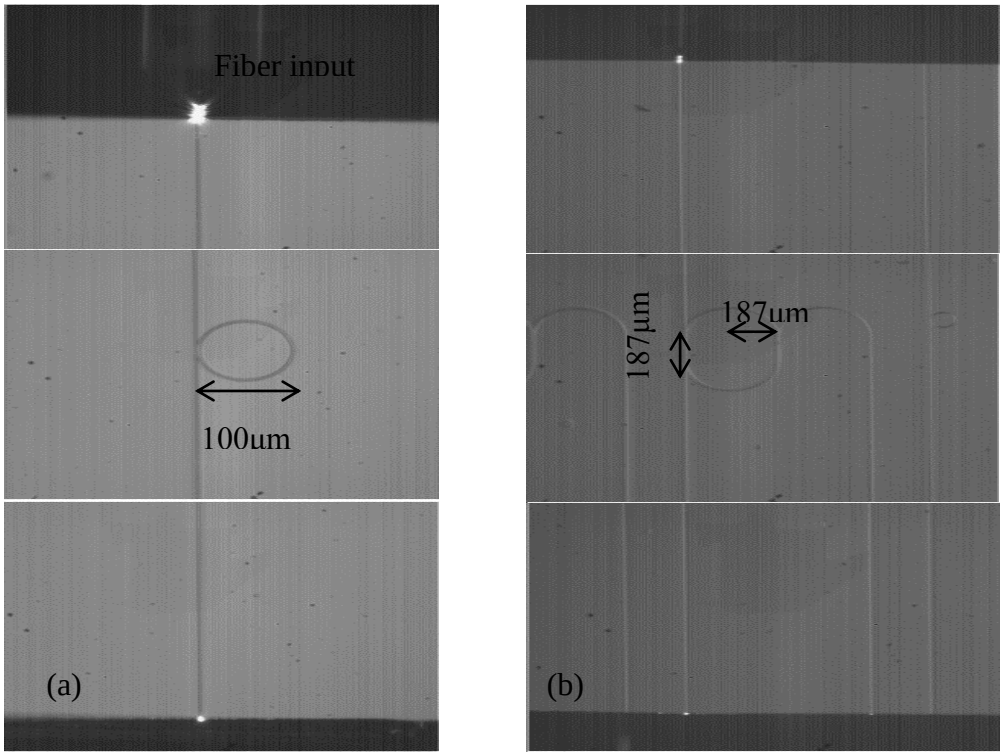

Figure 39. (a) The microring resonator seen under 20x magnification; (b) The 1.55 mm long racetrack resonator with an output port seen under 5x magnification

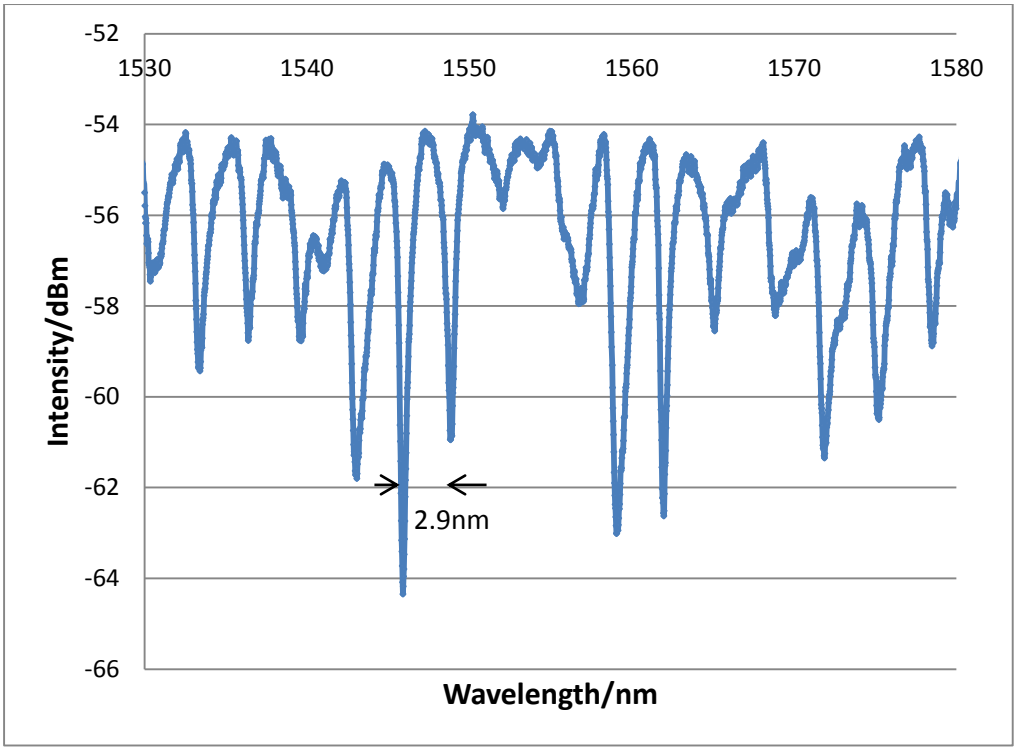

Figure 40. FSR on a 100 µm diameter ring resonator

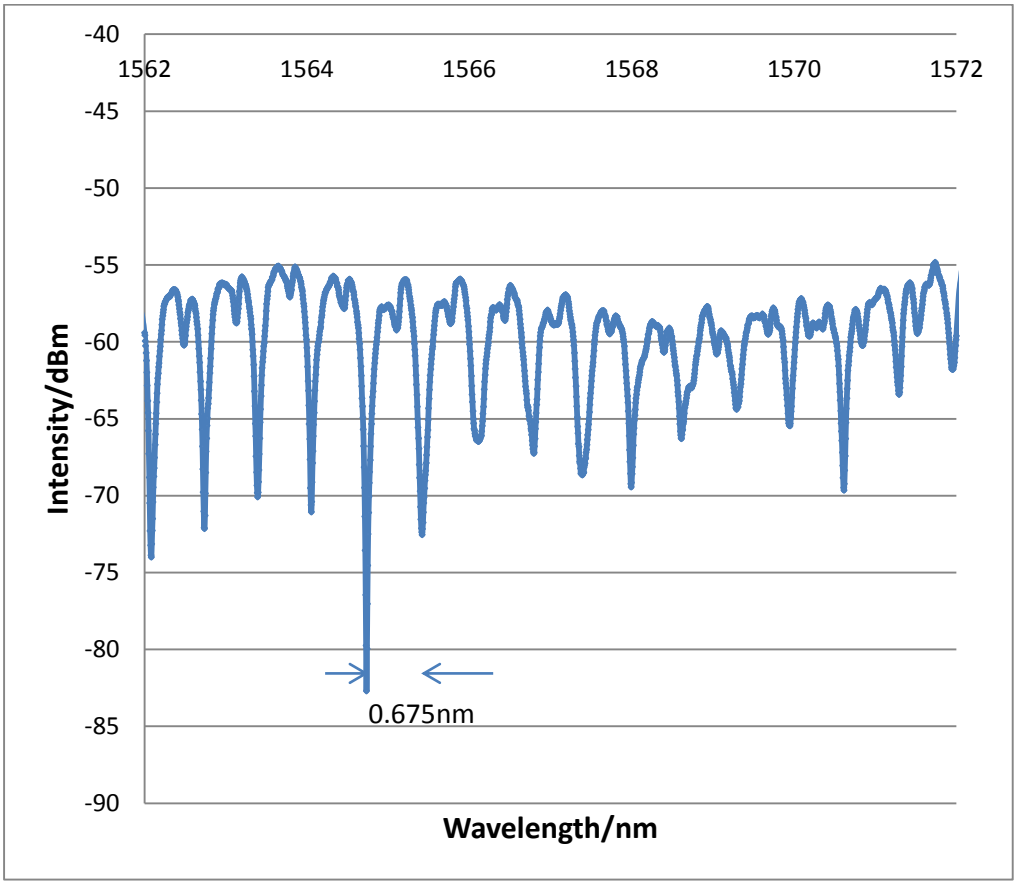

Figure 41. FSR of a 1.55 mm long racetrack resonator

Quality factors:

High Q-factor resonators are an essential component of microwave-optical modulators.

The resonance dip at the 1546nm wavelength is chosen for the quality factor measurement for the 104μm diameter microring resonator. The input power is 10mW, coupled into the waveguide using a lensed fiber (Fig. 40 (a)). A Lorentzian fit is done on the data, using the following formula.

$$L(x) = \frac{A}{(x - x_0)^2 + \left(\frac{1}{2}\Gamma\right)^2} + C \quad \text{(Equation 4)},$$

where Γ is the linewidth, and x_0 is the center wavelength. A and C are constants used in the Lorentzian fitting. From the linewidth, the Q-factor can be found as

$QF = x_0/\Gamma$ (Equation 5)

The microring resonator has a linewidth of 1.124nm, and a corresponding Q factor of 1376.

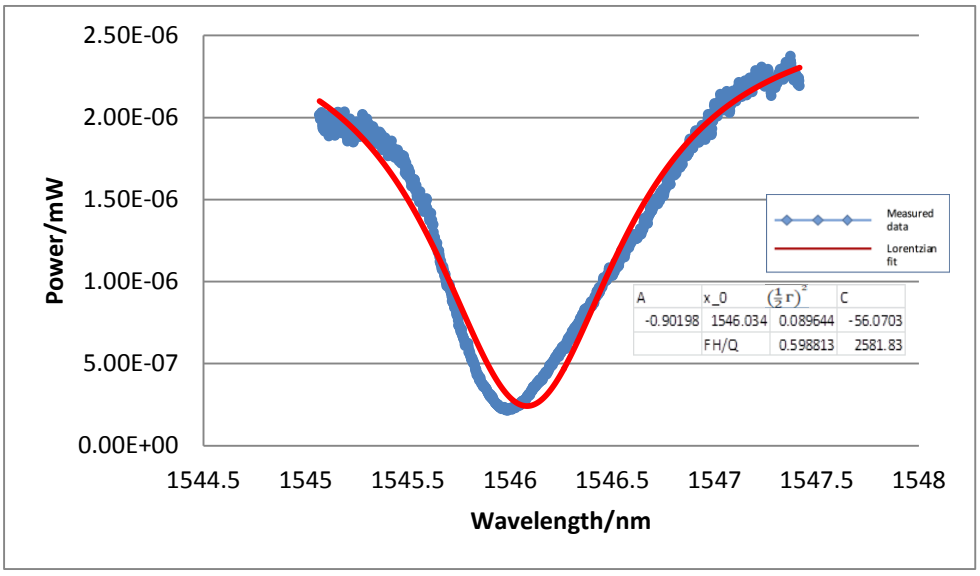

Figure 42. Q factor calculation at a resonant frequency of 1546 nm

The large racetrack resonators fabricated had a both a bus port and a drop port (Fig. 40(b)).

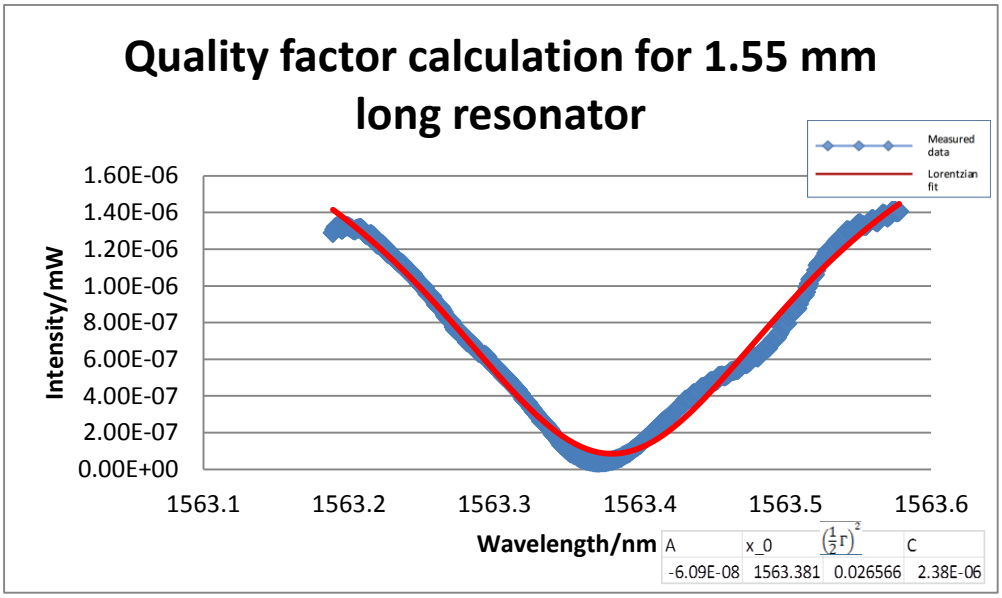

Figure 43. Q-factor calculation at a resonant wavelength of 1563.35 nm

The drop port was put there to double check the resonant peaks against the dips in the bus port. However, the intensity at the drop port was too low to be measured using our optical fiber. The presence of the drop port acted as another source for loss in the ring, and brought down the quality factor.

The linewidth was 0.326nm, which corresponded to a loaded Q factor of 4796, even with the drop port added.

This means that freestanding, weakly coupled racetrack resonators can potentially have quality factors higher than 5000. Although the QF has not yet reached the stage at which the racetracks can be used for microwave photonics experiments, they are a significant step towards that goal, and are good enough to be used in optical switches.

3.7 Summary

This chapter delineates the design and fabrication of photonic devices on lithium-niobate-on-insulator chips.

The chapter started with a detailed description of ridge and rib waveguide fabrication on the LNOI chips, the problems encountered in each step, and the steps taken to solve them. The rib waveguides were patterned using EBL, and etched physically through milling with argon ions. The waveguides at the beginning had rough sidewalls formed by the redeposition of lithium niobate, a problem which was solved through angled ion milling. The waveguides also had a sidewall angle varying from 50 to 70 degrees. The sidewall angle did not have a significant effect on the optical properties (3dB coupling length, splitting ratio, etc.) of the devices, which closely matched simulation results.

The waveguides were characterized in terms of their propagation losses. Two different techniques were employed for loss measurement. For waveguides with high scattering losses, the decrease in scattering intensity with distance was used to calculate the loss. For waveguides with low scattering loss, gratings were fabricated at the end of the waveguides at different lengths, and the relative intensities of the outcoupled light were used to calculate the propagation losses. The fabricated waveguides formed the foundation for the subsequent devices that were designed and fabricated.

Y-branch splitters and 3dB couplers were fabricated, whose performances closely matched simulations carried out in Rsoft's BeamPROP, a software that employs the beam propagation method. The results for this section of the thesis can be subsequently used in any project involving the design of a rib waveguide based MZI on LNOI chips.

Ring resonators and racetrack resonators were fabricated, and characterized in terms of their free spectral range and quality factors. Microring resonators, with 100 micron diameter were shown to have a quality factor in the order of 1000. Large, millimeter scale, racetrack resonators were fabricated, and were shown to have a loaded quality factor of over 4000.

The ring resonators and racetrack resonators fabricated using this process did not meet our expectations in terms of their quality factors. Q-factors in the order of 10^6 are needed in experiments involving microwave modulation. Focused ion beam milling based techniques have been used in recent years to get ring resonators with high quality factors in lithium niobate, but the techniques are not suitable for pattering large scale structures that are required by experiments in microwave photonics. The technique employed here to fabricate the millimeter-scale racetrack resonator can be further optimized to decrease the propagation and bending losses of the waveguides and improve the quality factors, and seems like a promising method to pursue for the fabrication of large scale resonators for microwave photonic experiments.

3.8 References

[1] G. Pobera, H. Hu, W. Sohler, and P. Gunter. "Lithium-niobate-on-insulator (LNOI) for micro-photonic devices." Laser and Photonics reviews, vol. 6, pp. 488-503, (2012).

[2] J. L. Jackel, R. E. Howard, E. L. Hu, and S. P. Lyman. "Reactive ion etching of $LiNbO_3$." Applied Physics Letters, vol. 7, p 1063 (1981).

[3] V. Dobrusin, and S. Ruschin. "Low-loss ridge Ti:$LiNbO_3$ waveguides fabrication." SPIE Proceedings, vol. 5577, (2014).

[4] F. Lacour, N. Courjal, M.-P. Bernal, A. Sabac, C. Bainier, M. Spajer. "Nanostructuring lithium niobate substrates by focused ion beam milling." Optical Materials, vol. 27, pp. 1421-1425, (2005).

[5] B. Weigand. "Fabrication of ridge waveguides in $LiNbO_3$." European conference on the Applications of Polar Dielectrics, pp. 1-4, (2012).

[6] J. Zhao, X. Liu, Q. Peng Liu, and X. Wang. "Lithium Niobate Ridge Waveguides Fabricated by Ion Implantation Followed by Ion Beam Etching." Journal of Lightwave Technology, vol. 28, pp.1913-1916, (2010).

[7] T. Wang, J. He, C. Lee, and H. Niu. "High-quality $LiNbO_3$ microdisk resonators by undercut etching and surface tension reshaping." Optics Express, vol. 20, p. 28119, (2012).

[8] X. Tong, "Characterization Methodologies of Optical Waveguides," Advanced Materials for Integrated Optical Waveguides. vol. 46, ed: Springer International Publishing, pp. 53-102, (2014).

[9] Y. Okamura, S. Yoshinaka, and S. Yamamoto, "Measuring mode propagation losses of integrated optical waveguides: a simple method," Applied Optics, vol. 22, pp. 3892-3894 (1983).

[10] I. P. Kaminow and L. W. Stulz, "Loss in cleaved Ti-diffused $LiNbO_3$ waveguides," Applied Physics Letters, vol. 33, pp. 62-64 (1978).

[11] R. Regener and W. Sohler, "Loss in Low-Finesse Ti" $LiNbO_3$ Optical Waveguide Resonators," Applied Physics B, vol. 36, pp.143-147, (1985).

[12] Y. Wang, S. Gao, K. Wang, and E. Skafidas. "Ultra-broadband and Low-loss Optical Power Splitter Based on Tapered Silicon Waveguides." IEEE Optical Interconnects Conference (OI), pp. 80-81, (2015).

[13] N. Zamhari, M. S. A. Rahman, N. H. Kamaruddin, A. A. Ehsan. "Analysis of Coupling Length for Symmetrical SOI Rib Waveguide." IEEE 5th International Conference on Photonics (ICP), pp. 56-58, (2015).

[14] D. Geuzebroek and A. Driessen, "Ring-Resonator-Based Wavelength Filters," Wavelength Filters in Fibre Optics. vol. 123, pp. 341-379, H. Venghaus, Ed., Springer Berlin Heidelberg, (2006).

[15] B. E. Little, S. T. Chu, H. A. Haus, J. Foresi, and J. P. Laine, "Microring resonator channel dropping filters," Journal of Lightwave Technology, vol. 15, pp. 998-1005, (1997).

[16] R. W. Boyd and J. E. Heebner, "Sensitive Disk Resonator Photonic Biosensor," Applied Optics, vol. 40, pp. 5742-5747, (2001).

[17] D.A. Cohen, M. Hossein-Zadeh, A.F.J. Levi. "High-Q Microphotonic electro-optic modulator." Solid-State Electronics, vol 45, pp. 1577-1589 (2001).

[18] V. S. Ilchenko, A. A. Savchenkov, A. B. Matsko, and L. M. "Whispering-gallery-mode electro-optic modulator and photonic microwave receiver." Journal of the Optical Society of America B, vol. 20, issue 2, pp. 333-342, (2002).

[19] H. Hu, F. Lu, F. Chen, B. R. Shi, K. M. Wang, D. Y. Shen. "Extraordinary refractive-index increase in lithium niobate caused by low-dose ion implantation." Applied Optics, vol. 40, pp. 3759-3762, (2001).

4. CONCLUSION AND FURTHER WORK

This thesis describes the fabrication of compact photonic structures on lithium-niobate-on-insulator chips. The project began with a long term goal: to fabricate devices with the potential to demonstrate nonlinear optical phenomena on chip. Two different techniques for the fabrication of waveguides on bulk lithium niobate were explored in detail, and it was concluded that the low index contrast of the devices fabricated rendered the techniques unsuitable for the fabrication of compact optical devices on lithium niobate.

Then, the focus was shifted to lithium-niobate-on-insulators. Fabrication techniques were tested and optimized and waveguides with losses lower than 5dB/cm were obtained. For nonlinear optical experiments to succeed, ring resonators with quality factors over 4,000,000 are required. Our techniques so far have been able to produce resonators with loaded quality factors of 5000.

In that regard, a lot has to be done in order to get high Q-factor resonators.

Directional couplers and 3dB splitters were designed and fabricated. The splitters and waveguides show promise, and can be utilized in the fabrication of ultra-compact MZIs.

The structures fabricated have the potential to be integrated into experiments in nonlinear optics and microwave photonics, and can also be employed in the fabrication of compact MZIs which can be used in optical data transfer.

The work done throughout the duration of this thesis has laid the groundwork for the fabrication of ultra-compact photonic devices on LNOI. But in order to culminate in something truly impactful, the work can be further expanded in the following areas.

Improving the sidewall angle of waveguides:

The waveguides fabricated through ion milling had sidewall angles varying from 50 to 70 degrees. This is because physical etching transfers the sidewall profile of the resist directly on to the substrate. To get more vertical sidewalls, a thicker layer of resist with a better selectivity can be used. Although we used MaN for our experiments, other EBL resists such as HSQ can be tried out to see if they have better sidewall profiles.

Employing photolithography to fabricate the devices:

Throughout the duration of the project, EBL has been used to pattern the resist on the wafers, because direct writing gave us a greater degree of freedom when optimizing device parameters. However, once the parameters for the final structures (width, splitter angles, coupling lengths, etc.) have been optimized, photolithography can be utilized to design the final device.

New method of propagation loss measurement in low loss waveguides:

The technique involving the use of diffraction gratings to outcouple light, followed by measuring their relative intensities, while gives a good estimate of the propagation loss of the waveguides, is subject to several sources of inaccuracies. For example, slight movements of the microscope objective might change the intensity of light captured, affecting the accuracy of measurement. In our experiments, the readings were taken several times to get an average value of the losses.

In order to get a better reading of the propagation losses, methods like the cut-back method or the Fabry Perot method can be employed.

Fabrication of an ultra-compact Mach Zehnder Interferometer on LNOI:

The fabrication techniques developed can be used to fabricate 2-micron wide rib waveguides on lithium niobate. These are about five times smaller in terms of width than waveguides formed by diffusion based techniques, and hence can have a higher field inside for the same applied voltage. An MZI fabricated with these waveguides would have a much smaller modulation length than MZIs formed by diffusion based techniques.

Microwave photonics experiments on chip:

Once the fabrication techniques have been optimized to yield high quality factor ($\sim 10^6$) resonators, they can be used in experiments in microwave photonics. As a proof of concept, the experiment performed by Cohen and Hossein-Zadeh (described in Section 1) can be replicated, with all the photonic components monolithically fabricated on a single chip.

5. APPENDICES

5.1 Appendix A: List of Publications

1. S. S. Yohanes, D. Jun, S. S. Saha, S. Hussain, M. Tsang and A. J. Danner. "Fabrication and characterization of microring resonators in titanium diffused lithium niobate", International Conference on Optical MEMS and Nanophotonics, pp.45-46, (2014).

2. S. S. Saha, S. S. Yohanes, D. Jun, M. Tsang, and A. J. Danner. "Photonic devices on lithium-niobate-on-insulator chips." Poster session presented at: Japan-Singapore International Workshop on Nanophotonics, Plasmonics and Metamaterials, (2014).

3. S. S. Yohanes, S. S. Saha, M. Tsang, A. J. Danner. "Rib microring resonators in thin film lithium niobate." 2015 International Conference on Optical MEMS and Nanophotonics, (2015).

4. S. Saha, S. S. Yohanes, D. Jun, A. Danner, M. Tsang. "Fabrication and characterization of optical devices on lithium-niobate-on-insulator chips." IEEE Photonics Global Conference, (2015).

5.2 Appendix B: The LNOI Chip Fabrication Procedure

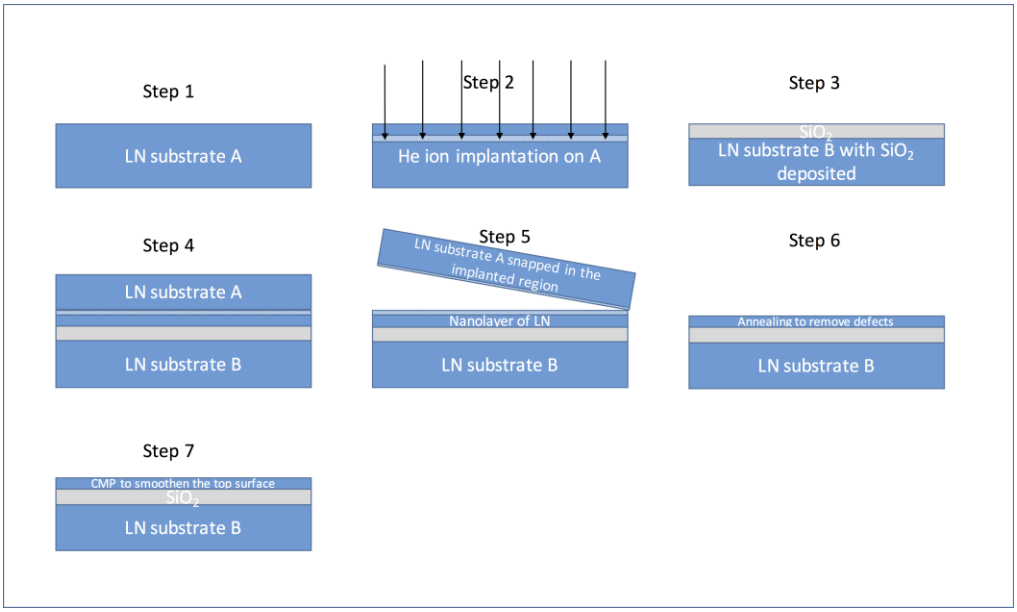

The schematic above illustrates the steps in the fabrication of lithium niobate on insulator (LNOI) chips that had been used in the course of this program. For our experiments, we purchased the chips from a company, NanoLN. But for the sake of completeness, I am outlining the procedure through which LNOI substrates are commercially fabricated.

Step 1: A lithium niobate substrate is cleaned to prepare it for ion implantation.

Step 2: The substrate is bombarded with He^+ ions with a dose of $4x10^{16}$ ions/cm^2. The ions create microdefects a few hundred nanometers below the surface of the LN. The depth at which the defects form can be controlled by controlling the implantation energy of the ions.

Step 3: A silicon dioxide layer is grown with plasma-enhanced chemical vapor deposition (PECVD) on another block of lithium niobate. The substrate is then annealed at 450^{o}C for eight hours to remove any residual gases, and the oxide layer is chemical-mechanically polished down to sub-nanometer roughness.

Step 4: The top surface of the ion implanted LN is attached to the SiO_2 layer by direct wafer bonding, and then annealed at around 190^oC to improve the bonding strength.

Step 5: Then the temperature is ramped up to 228^oC and kept at the temperature for two hours. The substrate splits along the ion-implanted layer.

Step 6: Annealing is done at 450^oC for 8 hours to remove any defects formed by ion implantation.

Step 7: The top LN layer is chemically mechanically polished down to 0.5nm roughness.

A more detailed account of the fabrication process can be found in reference 1 of Chapter 3.

Reference:

1. G. Pobera, H. Hu, W. Sohler, and P. Gunter. "Lithium-niobate-on-insulator (LNOI) for micro-photonic devices." Laser and Photonics reviews, vol. 6, pp. 488-503, (2012)

5.3 Appendix C: Refractive Index Measurement with Prism Coupling

To find out the refractive index change in X- and Z-cut wafers subsequent to proton exchange and titanium diffusion, prism coupling was required.

As we do not have a prism coupling setup, we sent our titanium diffused samples to France. Prof. Aaron Danner, in collaboration with Prof Elhadj Dogheche, used the Metricon 2010 system to measure the refractive indices of the slab waveguides we provided him.

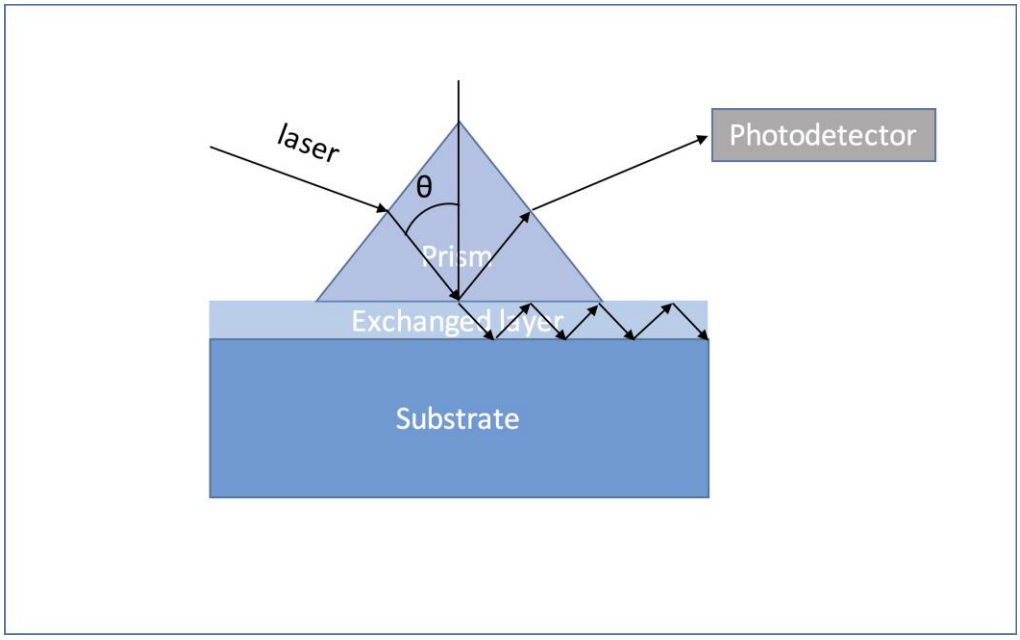

The setup is shown in the figure above. A prism coupler is pressed onto a sample on a rotation stage. Laser light is focused onto the prism and coupled into the sample. A photodetector measures the output light. As the stage rotates, the incident laser angle changes, and the reflected light intensity changes. The intensity of the resulting light radiating and reflecting from the surface provides information about the thin film substrate.

At certain discrete angles of incidence, the photons can couple into the film and enter into a guided optical propagation mode. This significantly reduces the

amount of light reflected into the photodetector. The angular location of the first mode (dip) determines the film index.

The results are tabulated below.

The following table shows the index measurement results for pure lithium niobate. For the most part, they confirm literature reported values.

Sample Type	Wavelength/nm	n_o measurements	n_e measurements
Z-cut, Pure Lithium Niobate	450	2.4786	2.2461
	633	2.2872, 2.2871, 2.2872, 2.2875	2.2024, 2.2024
	975	2.265, 2.2656 2.2352, 2.2679	2.2113
	1539	2.2112, 2.2119	2.14
X-cut, Pure Lithium Niobate	450	2.4766	
	633	2.2872, 2.2863, 2.2866, 2.2863, 2.2866	2.2024, 2.2022

The following table shows the refractive indices of proton exchange slab waveguides on lithium niobate.

Sample Type	Fabrication	Wavelength/nm	n_o measurements	n_e measurements
Z-cut APE slab	PE: 240^{o}C, 90 mins Anneal: 350^{o}C, 4 hours	633	2.2886 dn_o = 0.0014	2.2562 dn_e= 0.0536
X-cut APE channel	PE: 240^{o}C, 90 mins Anneal: 350^{o}C, 4 hours	633	2.2912 dn_o = 0.004	2.2128 dn_e=0.0104
		1539	2.2126	2.1431

The next table shows the refractive indices of titanium-diffused slab waveguides on lithium niobate.

Sample type	Fabrication	Wavelength/nm	n_o measurements	n_e measurements
Z-cut Ti:LN Slab Waveguide	1020°C 10 hours 40nm titanium	633	2.29 $dn_o = 0.0028$	-
X-cut Ti:LN Slab Waveguide	1020°C 10 hours 60nm titanium	633	2.2915 $dn_o = 0.0049$	2.2126 $dn_e=0.0102$
		1539	2.2126 $dn_o = 0.0014$	2.1431 $dn_e = 0.0031$
X-cut Ti:LN Slab Waveguide	1020°C 10 hours 80nm titanium	633	2.29 $dn_o = 0.00375$	2.2141 $dn_e = 0.0117$
		1539	2.2134 $dn_o = 0.0022$	2.1446 $dn_e = 0.0046$